DOI: 10.1002/smll.200700048

Environmentally Friendly Methodologies of Nanostructure Synthesis

*Yuanbing Mao, Tae-Jin Park, Fen Zhang, Hongjun Zhou, and Stanislaus S. Wong**

Various shapes of oxide and fluoride nanomaterials prepared by environmentally friendly techniques.

NANO MICRO small

From the Contents

Keywords:
- green chemistry
- hydrothermal synthesis
- molten-salt synthesis
- nanostructures
- template synthesis

small NANO MICRO

Environmentally friendly synthetic methodologies have gradually been implemented as viable techniques in the synthesis of a range of nanostructures. In this work, we focus on the application of green-chemistry principles to the synthesis of complex metal oxide and fluoride nanostructures. In particular, we describe advances in the use of the molten-salt synthetic methods, hydrothermal protocols, and template-directed techniques as environmentally sound, socially responsible, and cost-effective methodologies that allow us to generate nanomaterials without the need to sacrifice sample quality, purity, and crystallinity, while allowing control over size, shape, and morphology.

1. Introduction

Nanoscience is associated with the intimate understanding and control of matter at dimensions of roughly 1 to 100 nm and is intrinsically important because of the genuine expectation that the properties of materials at this scale will differ significantly from those of their bulk counterparts. Nanotechnology involves the imaging, measuring, modeling, and manipulation of materials at this length scale. We note that the term 'materials' appears in both of these conceptual definitions. It follows that the synthesis and fabrication of functional nanomaterials with predictive, rational strategies is a major focal point of research for many groups worldwide.

In practice, this effort has entailed the design, production, and characterization of a myriad of nanostructures including nanoparticles, nanocubes, nanorods, nanowires, and nanotubes, which maintain fundamentally interesting size-dependent electronic, optical, thermal, mechanical, magnetic, chemical, and other physical properties.[1–7] From the perspective of applications, these structures have wide-ranging utility in areas as diverse as catalysis, energy storage, fiber engineering, fuel cells, biomedicine, computation, power generation, photonics, pollution remediation, and sensing.[8–15]

In this century, it is apparent that the full potential of as-prepared nanostructures will only be realized when nanomaterials are not only synthesized in large quantities with reproducible size, shape, structure, crystallinity, and composition but also prepared and assembled using green, environmentally responsible methodologies.[16–18] The latter point is the focus of this Review and the social significance associated with developing these types of techniques cannot be overemphasized. Green chemistry can be broadly defined as the conscious reduction and/or elimination of hazardous starting materials, reactions, reagents, solvents, reaction conditions, and associated wastes in manufacturing processes. Specifically, in our laboratory, as with many other groups worldwide working on similar types of materials,[19–24] we have made a deliberate effort to abide by the following guidelines, that are generally atom economical and benign to the human health and environment,[25] in our synthesis of functional nanostructures:

1) Use of cost-effective, *nontoxic precursors*, if at all possible. Minimization of use of carcinogenic reagents and solvents (if possible, utilization of aqueous solvents). No experiments carried out with either pyrophoric, flammable, or unstable precursors.
2) Use of *relatively few* numbers of reagents.
3) *Minimization* of reaction steps – reduce waste, reagent use, and power consumption.
4) Development of reactions with *little if any byproducts* (if possible, high-yield processes with an absence of volatile and toxic byproducts).
5) Room-temperature (or *low-temperature*) synthesis under ambient conditions, if at all possible.
6) Efficiency of *scale-up*.

The main point of this analysis is that one can employ environmentally sound, socially responsible, and cost-effective methodologies without the need to sacrifice on sample quality, crystallinity, monodispersity, and purity. In fact, the methods that are routinely employed in our laboratory as well as in many others still allow us to reliably control the size, shape, and morphology, as well as monodispersity of our products.

It is worth noting that many as-prepared nanoscale materials in and of themselves are extremely useful from the point of view of environmental impact. For instance, nanoscale catalysts,[26–31] which are often reusable, promise not only milder and faster reaction conditions but also improved

[*] Dr. Y. Mao, T.-J. Park, F. Zhang, H. Zhou, Prof. S. S. Wong
Department of Chemistry
State University of New York at Stony Brook
Stony Brook, NY 11794 (USA)
Fax: (+1) 631-632-1703
E-mail: sswong@notes.cc.sunysb.edu
Prof. S. S. Wong
Condensed Matter Physics and Materials Sciences Department
Brookhaven National Laboratory, Building 480
Upton, NY 11973 (USA)
Fax: (+1) 631-344-3178
E-mail: sswong@bnl.gov

activity, greater selectivity, and higher product yields with overall lower volumes of waste. Nanofillers such as nanoclays can be used as additives in polymer composites, with the potential of replacing halogens and lead in fire retardants.[32] Nanoscale-derived products (including membranes, filters, and sorbents[33]) have the potential to desalinate water as well as to reduce the concentrations of toxic contaminants, such as metal ions, radionuclides, organic as well as inorganic solutes, to lower than parts-per-billion levels in surface water, groundwater, and industrial wastewater. Nanoparticle-based coatings[34] can be readily incorporated into scratch-resistant, nonstick surfaces without the necessity for either organic solvents or hazardous, volatile precursors.

In this Review, which is not meant as an exhaustive, comprehensive survey of the field, we choose to primarily focus on examples of technically sound, environmentally relevant methodologies of actually creating important nanostructures. Specifically, we focus on the application of these 'cleaner, greener' techniques (each with its own unique attributes) to the synthesis of nanoscale analogues of technologically significant transition-metal oxides and fluorides. We cover molten-salt synthesis in Section 2, hydrothermal processing in Section 3, and template synthesis in Section 4 with a special emphasis on the ongoing efforts in our laboratory. We also discuss potential device applications of nanostructured materials, prepared by these relatively facile methods, where applicable.

2. Molten-Salt Synthesis

The molten-salt synthesis (MSS) method is one of the simplest, most versatile, and cost-effective approaches available for obtaining crystalline, chemically purified, single-phase powders at lower temperatures and often in overall shorter reaction times with little residual impurities as compared with conventional solid-state reactions.[35] The environmental appeal of this technique arises from its intrinsic scalability, generalizability, and facility as well as its fundamental basis on the use of salt as the reaction medium. In fact, 1) the identity as well as the size of the anion associated with the salt, 2) the solubilities/dissolution rates of the constituent components within the molten salt itself, 3) the precise melting point of either the salt or complex salt mixture used, 4) the heating temperature and duration, as well as 5) the unique morphological (e.g., shape) and chemical composition of the precursors involved are all important, readily controllable factors that influence the growth rate as well as the resultant structural characteristics (i.e., size, shape, and crystallinity) of the as-prepared particles.[35–37]

The main processing stages associated with the MSS method are schematically illustrated in Figure 1.[37] Essentially, oxides and/or other appropriate precursors corresponding to the desired compound are mixed with either the desired salt (e.g., NaCl) or a eutectic mixture of salts (e.g., NaCl/KCl; $NaNO_3/KNO_3$) and then fired at a temperature above the melting point of the salt medium to form a molten flux. At this temperature, precursor molecules disperse, dissociate, rearrange, and then diffuse rapidly throughout the salt. Upon further heating, particles of the desired metal-oxide phase are formed through an initial nucleation step followed by a growth process that is very much dependent upon the identity of the salt species, the quantity of salt used in the reaction medium, the magnitude of the temperature at which the reaction is run, and the reaction duration. After cooling, the salt itself can be typically and rather simply eliminated by washing with deionized water. Upon drying, unagglomerated powders can be routinely obtained after appropriate processing.

While bulk materials have long been prepared using the MSS method, the preparation of uniform nanostructures

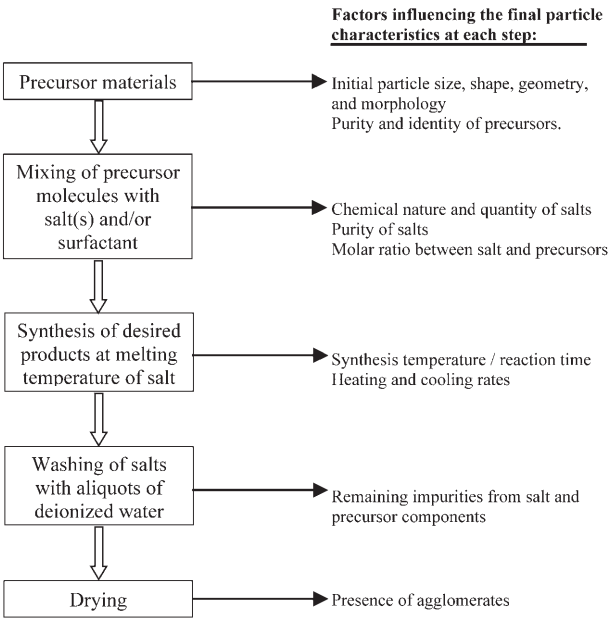

Figure 1. Flow chart illustrating factors influencing the molten-salt synthesis of transition-metal oxide materials. Adapted from Ref. [37].

Stanislaus S. Wong earned a BSc (first class honors) from McGill University in 1994 and completed his PhD thesis from Harvard University in 1999 under the tutelage of Prof. C. M. Lieber. After finishing a postdoctoral fellowship at Columbia University with Prof. L. E. Brus, he held the position of Assistant Professor in Chemistry at the State University of New York at Stony Brook with a joint appointment at Brookhaven National Laboratory (2000–2006), and was subsequently promoted to Associate Professor in September 2006. He and his group have wide-ranging interests in nanoscience including the rational chemical functionalization of carbon nanotubes, the synthesis and characterization of noncarbonaceous nanostructures (such as titanates, ferrites, fluorides, and zirconates), the development of synchrotron-based techniques for nanoscale characterization, and the use of probe microscopy to initiate localized chemistry. He has earned a National Science Foundation CAREER award, commencing in 2004, as well as an Alfred P. Sloan Foundation Faculty Fellowship (2006–2008).

NANO MICRO small

using this technique has only arisen relatively recently, that is, within the current century. Antonietti et al.[38] first described a 'convenient route for the synthesis of nanoparticulate salts, metals, and metal oxides' using concentrated salt solutions and block-copolymer surfactants. Research groups in Asia[39–43] demonstrated the high-yield preparation of smooth single-crystalline Mn_3O_4 (Figure 2), SnO_2, and CuO one-dimensional nanostructures through the MSS method using NaCl in the presence of a surfactant (such as Tween 80 or Triton X-100), and found that an Ostwald ripening mechanism (namely the dissolution of fine particles and redeposition onto larger particles) was primarily responsible for the nanowire growth observed. A few years later, Qian et al.[44] successfully synthesized Mn_5Si_3 nanocages and nanotubes through a molten-salt reaction between $MnCl_2$ and Mg_2Si at 650 °C by controllably altering reactant molar ratios as well as reaction temperatures.

In 2006, Wang and co-workers demonstrated the feasibility of a composite-hydroxide-mediated approach to the synthesis of single-crystalline complex oxide nanostructures of various structural and compositional motifs, based on a reaction between a metallic salt and a metallic oxide.[45] In addition, Ren and co-workers used a molten-salt-assisted thermal evaporation process to prepare aligned ultralong ZnO nanobelts, with an average length of 3.3 mm and widths up to 6 μm, stretching over a large area with the intention of creating electron sources with enhanced field-emission properties.[46] Furthermore, Jiao and co-workers were able to prepare a series of dispersed, crystalline $La_{1-x}Sr_xMnO_3$ nanoparticles using a molten-salt reaction in the presence of 2-pyrrolidone.[47] Over the years, our laboratory has applied this generalized methodology to the fabrication of transition-metal oxide nanostructures.

2.1. Perovskite Systems: $BaTiO_3$, $SrTiO_3$, $Ca_{1-x}Sr_xTiO_3$, $BaZrO_3$

Perovskite-type, ternary transition-metal oxides, with a general formula of ABO_3, are noteworthy for their advantageous dielectric, piezoelectric, electrostrictive, pyroelectric, and electrooptic properties with corresponding industrial applications in areas such as capacitors, actuators, high-k dielectrics, dynamic random-access memories, field-effect transistors, and logic circuitry.[48–50] These oxides, including $BaTiO_3$ and $SrTiO_3$, exhibit large nonlinear optical coefficients and large dielectric constants.[51] Because these effects are dependent on structure and finite size, considerable effort has been expended in the controllable synthesis of crystalline materials and of thin films of these ferroelectric oxides.[52–55]

Molten-salt synthesis[56] has been used to prepare pristine $BaTiO_3$ nanostructures (including nanowires) with diameters ranging from 50 to 80 nm and with aspect ratios ranging from 1 to larger than 25, as well as single-crystalline $SrTiO_3$ nanocubes with a mean edge length of 80 nm (Figure 3). MSS is a simple, readily scaleable (in terms of grams) solid-state reaction in the presence of NaCl and a nonionic surfactant, that is, NP-9 (nonylphenyl ether). The following reactions (Equations (1) and (2)) summarize a postulated mechanism for the synthesis of these nanomaterials. Here, the term 'M', the metal species, represents either Ba or Sr:

$$MC_2O_4 \rightarrow MO + CO + CO_2 \quad (1)$$

$$MO + TiO_2 \rightarrow MTiO_3 \quad (2)$$

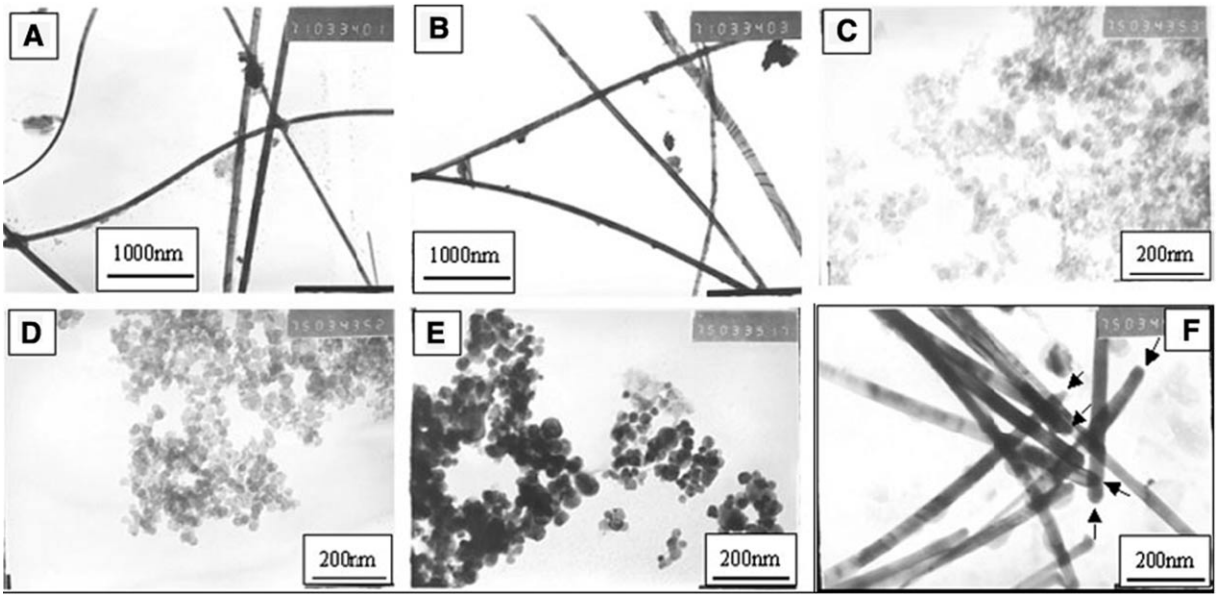

Figure 2. Transmission electron microscopy (TEM) images of A) Mn_3O_4 nanowires prepared by adding NaCl and NP-9 and gradually cooling to room temperature (RT), B) Mn_3O_4 nanowires prepared by adding NaCl and NP-9 and quickly cooling to RT, C) Mn_3O_4 particles prepared by adding NaCl only, D) Mn_3O_4 particles prepared by adding NP-9 only, E) Mn_3O_4 particles prepared from addition of neither NaCl nor NP-9. F) The tips of as-synthesized Mn_3O_4 nanowires. No spherical droplets were noted. Reprinted with permission from Ref. [41].

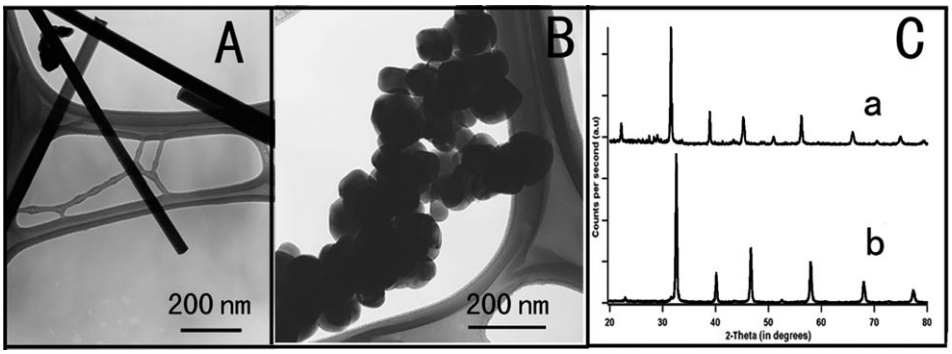

Figure 3. TEM image of A) as-prepared $BaTiO_3$ nanowires and B) as-prepared $SrTiO_3$ nanocubes. C) X-ray powder diffraction (XRD) patterns of a) as-prepared $BaTiO_3$ and b) $SrTiO_3$ samples.

The importance of the experimental conditions used to form these nanostructures cannot be underestimated. It is noteworthy that the use of different precursors, such as oxides and chlorides, as opposed to oxalates, produces neither phase-pure titanates nor even nanostructures. Moreover, even a slight change of conditions, such as running the reaction at a slightly lower temperature, that is, 810 °C (slightly below the melting point of NaCl), results in a lack of phase-pure titanates. The thermal effect can be rationalized by the change in the viscosity in the growth medium, which decreases when the temperature increases. That is, medium viscosity has an effect on the initial nucleation and subsequent diffusion of the growth species at the liquid–solid interface.[37,57]

Experimental results[56] also demonstrate that while maintaining identical experimental conditions (i.e., same ionic strength, temperature, and/or surfactant), but altering the metal precursor used, different shapes of perovskite nanostructures can be synthesized. These data are suggestive of the importance of interfacial energies between the constituents and the salt medium itself in determining the ultimate product morphology obtained. In fact, the shape of a nanocrystal is determined by the relative specific surface energies associated with the facets of the crystal. That is, with barium, nanowires can be fabricated whereas with strontium, nanocubes can be synthesized. The ultimate shape of a single-crystalline nanostructure reflects the intrinsic symmetry of the corresponding lattice. It is likely though that wires and cubes are kinetically dissimilar, morphological manifestations of the same underlying growth mechanism, involving the formation of initial nuclei of the cubic form.[58–60]

Because metallic conductivity in perovskites is due to the strong cation–anion–cation interaction, altering the structure of these materials through chemical substitution can have a dramatic effect on order and hence the properties of the resulting material. The $CaTiO_3/SrTiO_3$ system is a model example.[61–64] Strontium titanate is a cubic perovskite whereas calcium titanate is an orthorhombically distorted perovskite. In the combined $Ca_xSr_{1-x}TiO_3$ complex, where Sr^{2+} can be substituted for Ca^{2+} sites and vice vesra, the value of x has a dramatic effect not only on the dielectric constant but also on the phases of the material, which may range from orthorhombic to tetragonal to cubic.[65–67] Moreover, whether this material undergoes ferroelectric or antiferroelectric phase transitions depends on its exact chemical composition.[68]

Hence, the MSS method was used to prepare a series of single-crystalline $Ca_{1-x}Sr_xTiO_3$ $(0 \leq x \leq 1)$ nanoparticles.[69,70] The composition of the resulting nanoparticles is reproducibly tunable by adjusting the ratio of the reactants. Shapes of the generated $Ca_{1-x}Sr_xTiO_3$ nanoparticles alter from cubes to quasi-spheres with decreasing x values. Typical nanoparticles have sizes ranging between 70 and 110 nm, irrespective of the Sr or Ca content. The precise chemistry of the resulting nanoparticles is readily tunable by adjusting the ratio of the reactants, and this capability to generate materials of a desired doping level should enable future investigations of the composition-dependent properties of these materials. For instance, nanocubes of $SrTiO_3$, measuring 80 ± 10 nm, show strong first-order Raman scattering, unlike for bulk, and moreover, rapid polarization fluctuations within the nanoscopic ferroelectric regions in these materials interfere with a polar phonon, resulting in a Fano-like asymmetric line shape in these $SrTiO_3$ nanocubes as well as in $Ca_{0.3}Sr_{0.7}TiO_3$.[70]

Rational control over the actual shape of perovskite metal oxides has recently been achieved for single-crystalline $BaZrO_3$ particles through the MSS methodology using a NaOH/KOH salt mixture.[71] The evolution of particle morphology from predominantly cubes to a mixture of cubes and spheres and finally to solely spheres has been demonstrated by increasing annealing/reaction times at suitable annealing temperatures, all other parameters being equal. The sizes of the barium zirconate particles increased with increasing annealing time.

Based on a number of experiments (Figure 4), it was hypothesized that the conversion from cubes to spheres begins with the initial formation of cubes, that can be regarded as seed-particle motifs, once a critical particle size has been reached, for their subsequent morphological transformation to spheres. Moreover, the conversion rate (i.e., the percentage of spheres thereby generated from cubes) increases with increasing temperatures. That is, at sufficiently high annealing temperatures and/or overall reaction times conducive to cube conversion, sphere formation is favored 1) in samples annealed at high temperatures at a constant reaction time, and 2) in samples reacted for long periods of time at a constant annealing temperature. Not surprisingly, the greatest percentage of spheres was observed in the sample prepared at the highest annealing temperature of 720 °C and at the longest overall reaction times (350 min).

Rationally controlling the shape of perovskite oxides is of great importance due to their strongly structure-depen-

small NANO MICRO

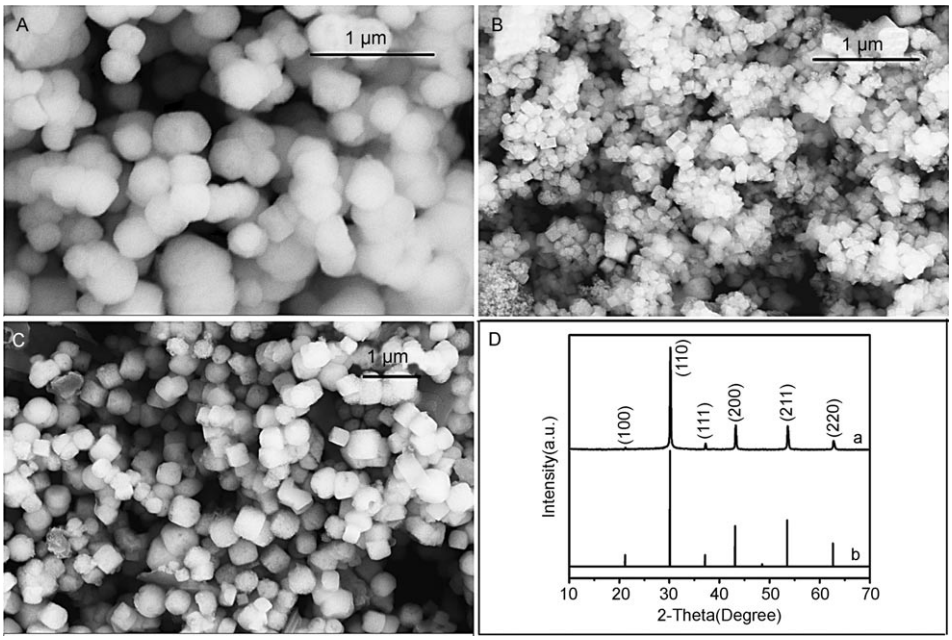

Figure 4. Scanning electron microscopy (SEM) images of $BaZrO_3$: A) spheres, B) cubes, C) mixtures of spheres and cubes. D) X-ray diffraction (XRD) patterns of $BaZrO_3$: as-prepared samples (a) and standard (b).

dent physical properties.[58,72,73] As-prepared, submicrometer-scale samples possessed a noticeably higher photoluminescence (PL) efficiency as compared with bulk, and in particular, spheres evinced a better PL signal as compared with cubes.

2.2. Fe-Based Nanostructures: α-Fe_2O_3, Fe/Fe_3O_4, $Bi_2Fe_4O_9$

The MSS technique,[74] with NaCl as the reaction medium, has also been used with respect to the large-scale production of single-crystalline α-Fe_2O_3 (hematite) rhombohedra from relatively polydisperse, polycrystalline and/or amorphous, commercially available starting precursor materials (Figure 5). By analogy with perovskites, shape control was demonstrated with these iron-based nanostructures as well. Rhombohedra represent a high-surface-area, anisotropic formulation of an industrially important material (iron oxide), which is an active component of gas sensors, pigments, advanced magnetic materials, photocatalysts, in addition to other types of catalytic materials.[75–78]

In a typical synthesis of submicrometer-sized (≈220nm), single-crystalline α-Fe_2O_3 rhombohedra, 0.5 and 20 mmol of iron oxide precursors and NaCl, respectively, were mixed thoroughly in an agate mortar. For elongated α-Fe_2O_3 structures, 1, 1.5, and 3 mmol of Fe_2O_3 along with 20 mmol of NaCl, respectively, were meticulously mixed, after which NP-9 was subsequently added. The resulting mixture was ground for at least 30 min prior to sonication for an additional 5 min, inserted into a quartz tube, heated at a ramp rate of 5 °C per min up to an annealing temperature at 820 °C for 3.5 h, and cooled thereafter to room temperature. As-prepared material was subsequently washed several times with distilled water, collected by centrifugation, and dried at 120 °C in a drying oven.

Furthermore, these as-prepared hematite structures could be transformed in situ into a nanoscale composite of Fe (iron) and Fe_3O_4 (magnetite) containing both hard and soft magnetic phases juxtaposed within one discrete, monodispersed anisotropic rhombohedral structure (Figure 5B). Briefly, the as-prepared hematite product was heated in a tube furnace at 360 °C for 5 h under a continuous flow of 5% H_2 in N_2. After the gas flow was stopped, the resulting product was subsequently heated in air to 240 °C for 2 h, cooled to room temperature, and then collected without further treatment. Magnetic properties measured for both precursor and product rhombohedral structures showed the expected presence of a Morin transition[79] as well as a Verwey transition[80] at a temperature of 252 K and 135 K (Figure 5 C and D), respectively. Nanostructured magnetic materials such as the Fe/Fe_3O_4 composite described herein have potential applications as ferrofluids, high-density magnetic recording media, and catalysts.[81] Moreover, the Fe/Fe_3O_4 composite has been utilized in environmentally significant processes, including as a heterogeneous Fenton's reagent for the removal of harmful organic pollutants such as halogenated hydrocarbons (e.g., trichloroethylene and tetrachloroethylene) from soils.

With respect to catalysts, it is noteworthy that the catalytic potential of $Bi_2Fe_4O_9$ for ammonia oxidation to NO is of current interest as these iron-based materials may likely replace current, irrecoverable, and costly catalysts based on platinum, rhodium, and palladium.[82,83] To this end, the MSS fabrication of discrete single-crystalline submicrometer-sized $Bi_2Fe_4O_9$ cubic structures as well as their elongation into orthorhombic and rod-like structures (Figure 6) has been reported.[84] In the associated experiments, the roles of surfactant, salt, precursor identity, as well as alterations in the molar ratio of Bi^{3+} to Fe^{3+} precursors, were systematically examined and correlated with the predictive formation of different shapes of $Bi_2Fe_4O_9$ products. For instance, as-prepared $Bi_2Fe_4O_9$ structures, prepared using a 3:1 molar ratio of Bi_2O_3 to Fe_2O_3, mainly consisted of orthorhombic structures composed of smooth surfaces, showing some slightly truncated corners or edges. The mean lengths of the shorter and longer edges of the rectangular structures were measured to be 662 ± 181 and 1043 ± 350 nm, respectively. By contrast, typical morphologies of the $Bi_2Fe_4O_9$

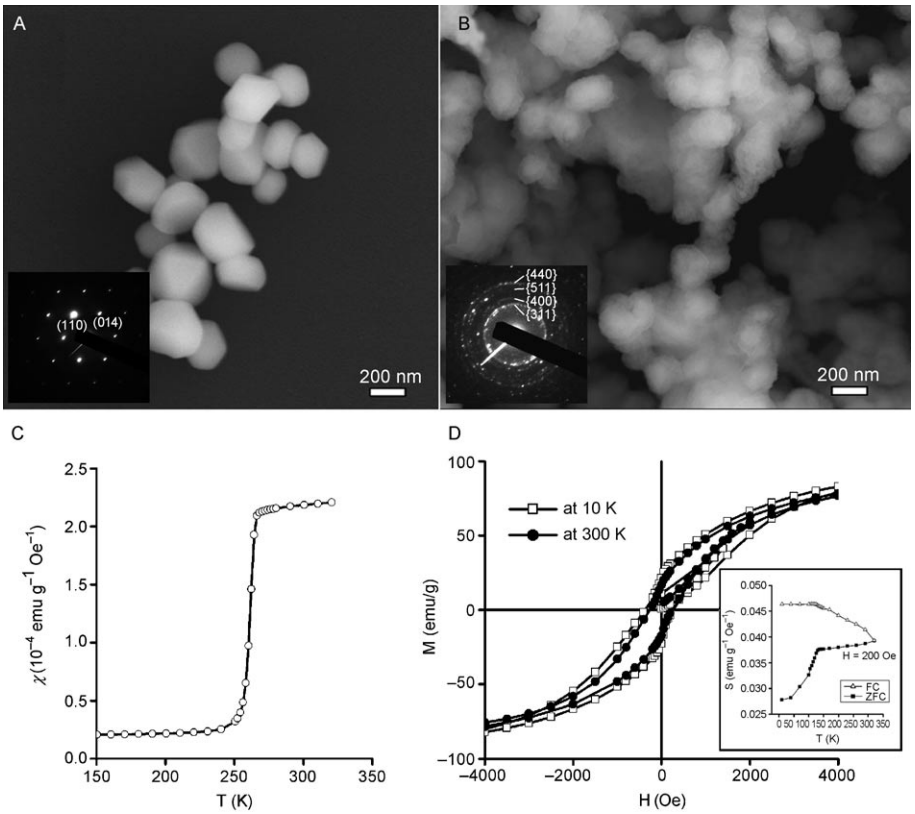

Figure 5. A) SEM image of as-prepared hematite (α-Fe_2O_3) rhombohedra particles. The inset shows their corresponding selected-area electron diffraction (SAED) pattern. B) SEM image of as-transformed magnetic composites of iron (Fe) and magnetite (Fe_3O_4). The inset shows the corresponding SAED pattern. C) Temperature dependence of the magnetic susceptibility for hematite rhombohedra, showing zero-field cooling (ZFC) curves, with an applied magnetic field set at 200 Oe. The Morin transition temperature observed for hematite rhombohedra was 252 K. D) Hysteresis loops at 10 K and 300 K repeatedly of as-transformed Fe/Fe_3O_4 composites. The kink observed at low field reveals magnetization reversal of the soft magnetic phase.[9] The inset shows the temperature dependence of the magnetic susceptibility for the Fe/Fe_3O_4 composite, showing ZFC (■) and field-cooling (FC, △) curves, with an applied magnetic field set at 200 Oe. The Verwey transition temperature is observed at 135 K.

structures, derived from a 6:1 (Bi^{3+}:Fe^{3+}) molar ratio of precursors, mainly consisted of smooth, straight, and rodlike structures. The lengths of these rods attained $\approx$10 μm with an average width of only a few micrometers.

Experimental observations confirmed that there is only a very narrow permutation of experimental parameters such as a) a 1:1 molar ratio of precursors, b) the addition of salt (i.e., NaCl), c) the presence of surfactant (i.e., Igepal CO-630 or NP-9 surfactant), and d) the usage of specific elemental precursors, that collectively will yield single-crystalline $Bi_2Fe_4O_9$ cubes with predictive control of shape and size. A typical mean edge length of as-prepared cubes obtained was 386 ± 147 nm, and the faces were essentially flat. The presence of surfactant may prevent interparticle aggregation by forming a "shell" around individual particles.[85] In addition to structural characterization of $Bi_2Fe_4O_9$ cubes using microscopic means, Mössbauer and superconducting quantum-interference device (SQUID) measurements (Figure 6) respectively revealed the presence of two different iron subsites, that is, a tetrahedral and an octahedral one, and showed a slightly lower Néel temperature (T_N) of the cubes (250 K) as compared with that of the bulk (263 K).

3. Solvothermal/Hydrothermal Processing

Relatively environmentally sound, lower-temperature solution-based methods also exist for nanostructure formation. For instance, when a solvent is heated in a sealed vessel (such as an autoclave or a bomb calorimeter-type apparatus) so that the autogenous pressure far exceeds the ambient pressure, this technique allows for solvents to be brought to temperatures well above their boiling points.[86] Performing a chemical reaction for the preparation of inorganic solids under such conditions is referred to as solvothermal processing. In the specific but more common case where water is used as the solvent, this technique is defined as hydrothermal processing.

The key to hydrothermal/solvothermal synthesis is that it exploits the measurable solubility and reactivity of almost all inorganic substances in solvents at elevated temperatures and pressures, thereby permitting the subsequent crystallization of the dissolved material/precursor ions from solution under these conditions.[87,88] In fact, because the properties of the solvent mixture as well as those of the reactants differ intrinsically under these special experimental conditions from their corresponding properties under ambient conditions, the net result is that this type of processing allows for greater manipulation of a larger suite of experimental variables in the synthesis of high-quality nanomaterials. Hence, there are complex structure–synthesis relationships that exist with hydrothermal/solvothermal processing, a point made very clearly in recent work associated with the design of polyoxometalate-based integrated nanosystems.[89]

In general, reaction temperatures (from close to room temperature to as high as a few hundred degrees Celsius), reaction times, pH values, solvent choice and concentration, the presence of additives, and the use of different autoclave geometries are all parameters that can be readily altered in hydrothermal/solvothermal processing.[88,90,91] As an illustration of the critical importance of parameter selection, dispersible, high-quality Te nanowires, possessing a diameter range of 4–9 nm and characterized by a strong blue/violet luminescent emission, can be generated hydrothermally

NANO MICRO small

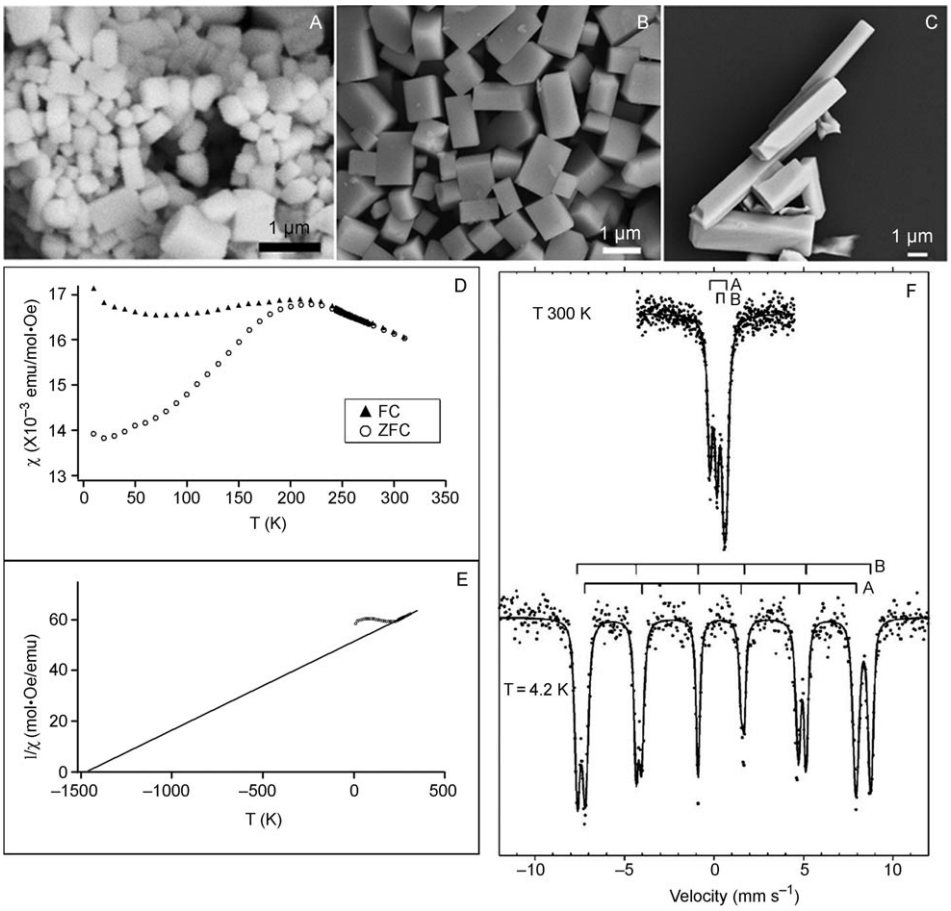

Figure 6. SEM images of $Bi_2Fe_4O_9$: A) cubic, B) orthorhombic, C) rodlike structures. D) The temperature dependence of the magnetic susceptibility for $Bi_2Fe_4O_9$ cubes, showing ZFC (○) and FC (▲) curves with an applied field set at 1000 Oe. T_N observed for the cubes is at a temperature below 250 K. E) The inverse magnetic susceptibility (○) and fit of the Curie–Weiss law, $x = C/(T-\theta)$, above T_N (solid line) to the experimental data for $Bi_2Fe_4O_9$ structures. F) Mössbauer spectra of $Bi_2Fe_4O_9$ cubes at 300 K and 4.2 K. Solid lines are least-square fits to experimental points, assuming a superposition of two different iron subsites, that is, a tetrahedral (bar diagram A) and an octahedral (bar diagram B) one.

only in the presence of poly(vinylpyrrolidone) under mild conditions.[92] Moreover, the stepwise formation of as-prepared products, generated by systematically varying parameters governing hydrothermal crystallization processes, has, in general, been monitored in situ using atomic force microscopy, electron microscopy, diffraction techniques, as well as probes of local structure such as XANES, EXAFS, and NMR.[89] Current efforts have focused on combining several of these techniques with the ultimate goal of understanding the precise mechanism of structure control (such as shape, size, and aspect ratio) in oxide systems produced hydrothermally. As an illustration of shape dictation using this method, hematite nanocubes[93] with a broad size distribution, which were found to be superparamagnetic at room temperature, can be synthesized by decomposition of an iron–oleate complex under hydrothermal conditions.

What is environmentally significant about this methodology is that the solvothermal/hydrothermal processes allow for inorganic materials to be prepared at temperatures substantially below those typically associated with traditional solid-state reactions. Moreover, unlike for coprecipitation and sol–gel types of reactions, which also occur at relatively reduced temperatures, the products of solvothermal/hydrothermal reactions are typically crystalline and tend not to require post-annealing treatments. Finally, solvothermal reactions are considered to be advantageous with additional benefits including reaction yields approaching 100%, facility of experimental setup, relatively low costs for reagents, and relatively short reaction times.[2]

Not surprisingly, different types of nanomaterials, such as but not limited to MnO_2, $Mg(OH)_2$, $CdWO_4$, $LaCrO_3$, ZrO_2, $Y_2Si_2O_7$, Sb_2S_3, PbS, Ni_2P, Bi, and SnS_2 nanotubes in addition to nanowires of MoO_3, Bi_2S_3, $BaMo_2O_7$, single-crystalline silver molybdate/tungstate, alkali/alkaline-earth molybdate, mixed ammonium molybdenum/tungsten bronze, lanthanide hydroxide, Cu_2O, and SiC, have been successfully synthesized under solvothermal/hydrothermal conditions.[2,87,94–103] It is believed that the spontaneous formation of single-crystalline nanotubes/nanowires without the aid of templates is based on a 'rolling' mechanism in which layered compounds, held together by weak van der Waals interactions, serve as intermediates for the formation of nanotubes/nanowires;[104] in this model, the inherent, intrinsic crystal structure as well as the laminar nature[105] of the precursor materials and metals are determinant factors governing the growth, size, and composition of the resulting one-dimensional nanostructures.

In addition, uniform $V_2O_5 \cdot x\,H_2O$ nanobelts (micrometers long, 100–150 nm wide, and 20–30 nm thick) as well as their ultralong nanoroll analogues[106] have been synthesized on a large scale using a simple hydrothermal growth route involving a vanadate precursor in the presence of different acids at 180 °C for 24 h; in that case, the morphologies and compositions of the synthesized products had a distinctive effect on their electrochemical intercalation properties and photocatalytic activities, highlighting the importance of developing controlled synthesis protocols. Moreover, oxide@C core/shell nanostructures, that is, containing carbonaceous polysaccharide shells and oxide cores, have been synthesized hydrothermally at 180 °C for 4 h and subsequently converted

into metal@C core/shell structures with unusual reversible Li-storage capabilities.[107] More complicated architectures such as ZnO flowers,[108] composed of either branched spindles or prismatic whiskers with flat ends, have also been synthesized by hydrothermal treatment of $Zn_3(OH)_2V_2O_7{\cdot}H_2O$ nanosheets in aqueous sodium hydroxide solution at 120 °C without the use of either a surfactant or a microemulsion; the effects of varying basicity, temperature, and reaction time were studied with respect to the formation of these structures.

Nonetheless, nanocrystals prepared according to this technique typically are polydisperse in terms of their size and shape distributions. Hence, to rectify this problem, we and other laboratories are exploring a number of strategies including a) using a combination of solvothermal/hydrothermal processes coupled with a reverse micelle technique, as well as b) tuning parameters such as solvent pressure, temperature, reaction time, and the molar ratio of precursors in order to simultaneously optimize both nucleation rate as well as size monodispersity. For instance, Colvin and coworkers reported the synthesis of nanoscale quartz by a hydrothermal treatment involving amorphous silica precursors followed by pH-controlled dialysis, filtration, and centrifugation steps, a protocol that can generate crystalline particles ranging in sizes from 10 to 100 nm.[109] The key in all of these strategies has been to create distinctive, well-separated nucleation and growth phases.

Recently, two relatively new modifications[86] to solvothermal/hydrothermal syntheses have appeared, described as 1) flow-hydrothermal techniques and 2) microwave-solvothermal reactions, respectively. In the first method, a preheated solvent is mixed with reactants prior to introduction into a heated chamber whose pressure is controlled using a back-pressure regulator; reactants are pumped in using high-pressure pumps typically used in high-pressure liquid-phase chromatography. The continuous nature of this particular process is amenable to desirable, large-scale production and has already been applied to CeO_2–ZrO_2 solid solutions.[110] The second method, that is, microwave-hydrothermal processing,[111] employs polymeric bombs/autoclaves that are transparent to microwaves and whose aqueous contents would correspondingly couple and rapidly heat up to a temperature that is governed by pressure. Komarneni and co-workers,[112] in particular, made extensive use of this method to synthesize a wide variety of compounds and composite materials, such as nanoparticles of MFe_2O_4 (M = Zn, Ni, Mn, Co) ferrite. Other recently reported nanophase compounds prepared by this combined microwave-hydrothermal technique include Fe_3O_4, ZrO_2, and $Ce_{0.75}Zr_{0.25}O_2$.

3.1. Titanate and Titania Nanostructures

3.1.1. $BaTiO_3$, $SrTiO_3$ Nanotubes

Our initial foray into this area of synthesis was inspired by previously reported hydrothermal syntheses of ceramic powders,[113–116] especially barium titanate. Typically, these reactions allow for the preparation of relatively phase-pure products under low temperatures and with control over reaction conditions such as concentration, pH, and temperature. Previous reports[117–119] focused on the reaction of a barium precursor such as $Ba(OH)_2$ with a titanium source such as titanium alkoxide, titanium tetrachloride, titanium oxide powder, or a titanium oxide gel. An initial, hydrothermally inspired strategy was to utilize a titanium oxide (TiO_2) nanotube as a bona fide precursor material itself in order to generate barium titanate and strontium titanate nanotubes in a rational manner.

Hence, TiO_2 nanotubes were prepared initially as described in published procedures.[120,121] Briefly, anatase powder was dissolved in an aqueous NaOH solution in a Nalgene flask, refluxed over an oil bath for 20 h with stirring, separated from solution by centrifugation, and ultimately washed until the supernatant attained a pH value less than 6. Subsequently, in a typical reaction to generate $BaTiO_3$ and $SrTiO_3$ nanotubes respectively, a mixture of either $Ba(OH)_2$ or $SrCl_2$ and the generated TiO_2 nanotubes (with an initial molar ratio of 1:1) was combined under Schlenk conditions (i.e., in the presence of an inert atmosphere so as to exclude air, especially CO_2, and moisture), after which the reaction mixture was refluxed over an oil bath for 20–60 h under high pH conditions while stirring under a continuous stream of argon or nitrogen.

The main problem with this synthesis was that whereas the collected data were consistent with the presence of the desired barium titanate and strontium titanate products,[122] powder X-ray diffraction patterns showed small traces of unreacted TiO_2 and carbonate byproducts. This problematic result as well as further attempts at experimental optimization led to the reasonable conclusion that the initial preparation of TiO_2 nanotubes was actually much more complicated than previously believed. In fact, it was unlikely to be governed by a simple 'rolling' formation mechanism, and that belief inspired efforts to more fully explore the reproducible synthesis of these structures through the formation of alkali-metal titanate intermediates.

3.1.2. Three-Dimensional (3D) Nanostructures of Sodium Hydrogen Titanate, Hydrogen Titanate, and TiO_2

It is worth considering the importance of these types of materials. In general, alkali-metal titanates can be delaminated to form exfoliated nanosheets, which are useful a) as building blocks for new materials such as nanocomposites containing bulky guest molecules such as organic polymers, polyoxocations, and biocatalytic hemoglobin,[123] and b) as ion exchangers and photocatalysts.[124] Titanium oxide, a wide-bandgap semiconductor, has been utilized as components of batteries, photocatalytic materials, pigments, cosmetics, optoelectronic devices, and gas sensors.[125–127] Titanate and titania nanotubes, nanowires, and nanoparticles are particularly interesting because their catalytic activity and their sensitivity to hydrogen, as examples of highly desirable properties, are dependent upon their inherent crystal structure, particle size, surface area, and porosity.[127,128] As a result of the wide range of valuable functional properties associated with these materials, it was very important to ra-

NANO MICRO small

tionally control the size, morphology, and assembly of titanate and titania nanostructures and to develop strategies for their large-scale syntheses.[129–131]

As such, the observation that either sodium or potassium hydrogen titanate one-dimensional (1D) nanostructures, measuring several hundreds of nanometers in length and up to several nanometers in diameter, could be efficiently and facilely organized in situ into hollow 3D micrometer-scale spherical aggregates or urchin-like structures, under a variety of reaction conditions (including temperature variations[129]) was both encouraging and promising. Indeed, these hierarchical structures were produced using a general redox strategy combined with a hydrothermal reaction involving a titanium source (e.g., either Ti foil or Ti powder), a basic NaOH or KOH solution, and an oxidizing H_2O_2 solution. To illustrate the generalizability of this protocol, 3D urchin-like structures of γ-MnO_2 have been previously prepared[132] using a similar hydrothermal method based on the reaction between $MnSO_4$ and $KBrO_3$ at temperatures of 110 to 130 °C.

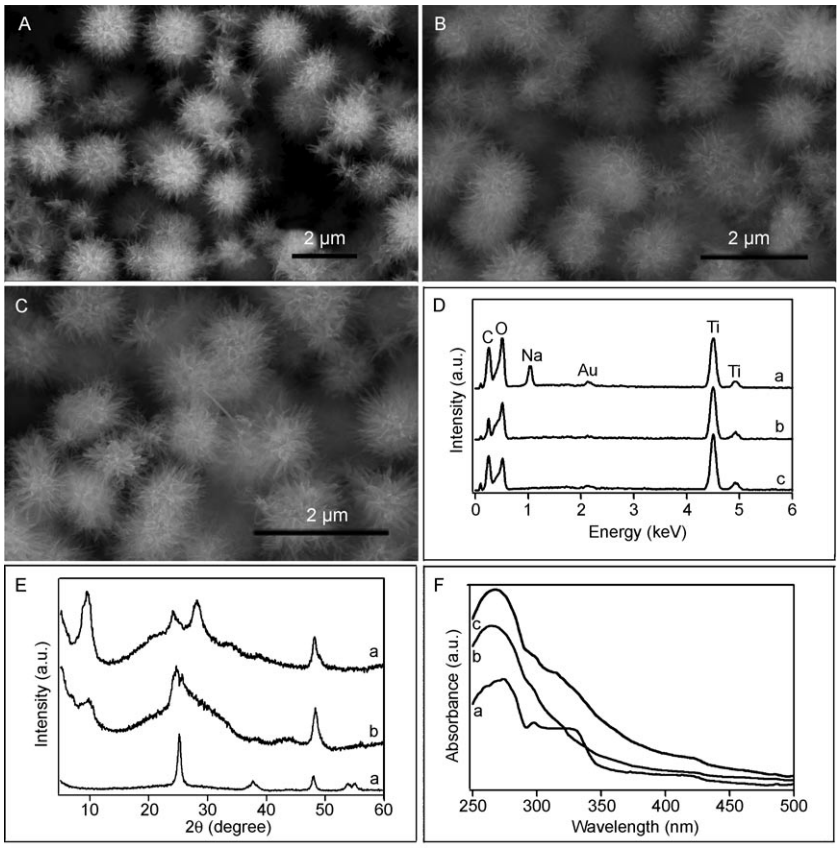

Figure 7. SEM images of as-prepared powders of hollow micrometer-scale spherical 3D assemblies of 1D nanostructures: A) sodium hydrogen titanate, B) hydrogen titanate, C) anatase TiO_2. D) Energy dispersive X-ray spectroscopy (EDS), E) XRD, and F) UV/Vis data of as-prepared powders of hollow micrometer-scale 3D spherical assemblies of 1D nanostructures: a) sodium hydrogen titanate, b) hydrogen titanate, c) anatase TiO_2. Low-intensity Au peaks in the EDS spectra originate from the gold coating used to eliminate charging effects prior to SEM imaging with the C peaks arising from the underlying conductive carbon tape.

It should be noted that these one-pot assembly processes did not involve the use of sacrificial templates to render spatial confinement, which tend to yield amorphous or semicrystalline products.[133] Moreover, the surfactant-free synthetic methodology of hierarchical structures of the 1D nanostructures reported was a simple, inexpensive, and mild synthetic process. In addition, the initially formed assemblies of alkali-metal hydrogen titanate 1D nanostructures could be subsequently transformed into their analogous anatase TiO_2 1D nanostructures by merely annealing the intermediate hydrogen titanate 1D nanostructures in air. Furthermore, the reported protocol for the controlled synthesis of assemblies of 1D nanostructures of titanates and anatase could be easily scaled up to achieve gram quantities of product in a simplistic manner, without loss of structure.

Typically, as-prepared 3D assemblies (Figure 7) of titanate and titania 1D nanostructures had overall diameters ranging from 0.8 μm to 1.2 μm, while the interiors of the aggregates were hollow with a diameter range of 100 to 200 nm, resembling the microscopic variant of a sea urchin with spines.[134] The component, constituent titanate and anatase titania 1D nanostructures had a diameter range of 7 ± 2 nm and possessed lengths of up to several hundred nanometers. A proposed two-stage growth mechanism, involving the initial formation of primary 1D nanostructures that subsequently self-assembled into hollow micrometer-scale 3D spheres was supported by time-dependent scanning electron microscopy, atomic force microscopy, and inductively coupled plasma atomic emission spectrometry data.

What the results (Figure 7) conclusively showed in this experiment was that pure anatase TiO_2 nanostructures could not be directly formed hydrothermally without the mediation of hydrogen titanate. That is, anatase TiO_2 nanostructures could not merely be formed via a simple one-step alkaline-mediated hydrolysis process; rather the work suggested that anatase synthesis involved a much more complex protocol, necessitating the initial formation of sodium/potassium hydrogen titanate, neutralization of that species to hydrogen titanate, and ultimately conversion to titania. What is equally significant is that from X-ray diffraction and Raman results, it was shown that the hydrogen titanate species actually consisted of an orthorhombic lepidocrocite-type ($H_xTi_{2-x/4}\square_{x/4}O_4$ ($x \approx 0.7$, □: vacancy)) titanate structure. Only a subsequent high-temperature annealing treatment in air at 350 to 500 °C for 1–10 h and an accompanying dehy-

dration process could transform these assemblies of 1D hydrogen titanate nanostructures into their anatase titania analogues without atom-by-atom recrystallization of anatase.[135]

These anatase titania assemblies were also found to be active photocatalysts for the degradation of synthetic Procion Red dye, a model system for organic pollutants, under UV-light illumination. Thus, the high-quality, micrometer-scale, urchin-like structures with their large surface-area-to-volume ratio could be expected to be incorporated as components of a number of devices including photonic instruments and dye-sensitized solar cells.

3.2. Transformation of Nanosized Titanate into Analogous TiO_2 Nanostructures

As an extension of this study (Figure 8), the size and shape dependence of a number of hydrothermally prepared titanate nanostructure 'reagents'[121,129] were analyzed with respect to the controllable preparation of anatase TiO_2 (titania) products by a reasonably mild hydrothermal process coupled with a dehydration reaction.[136] In these experiments, titanate nanowires and nanotubes were converted and transformed into anatase titania nanowires and nanoparticles, respectively, at essentially 100% yield under neutral aqueous and relatively low-temperature conditions, unlike the acidic aqueous conditions used by Zhu et al.[131] In fact, it was shown that the size and shape of the precursor titanate structural motif strongly dictated and essentially controlled the eventual morphology of the resulting titania products. Conceptually, this approach has implications for nanoscale design as well as for the probing of morphology-dependent properties in nanomaterials.

Specifically, in this work (Figure 8),[137] protonic lepidocrocite titanate nanotubes (prepared at 120 °C under hydrothermal conditions) with diameters of ≈10 nm were transformed into exceptionally high-purity anatase nanoparticles with an average size of 12 nm. Lepidocrocite hydrogen titanate nanowires (prepared under hydrothermal conditions at 180 °C) with relatively small diameters (average diameter range of ≤200 nm) were converted into single-crystalline anatase nanowires with relatively smooth surfaces. Larger diameter (>200 nm) titanate nanowires (similarly prepared under hydrothermal conditions at 180 °C) were transformed into analogous anatase nanowire motifs, resembling clusters of adjoining anatase nanocrystals with perfectly parallel, oriented fringes; a spontaneous self-aggregation of particulate building blocks has been used to explain the analogous formation of $ZnWO_4$ nanorods[138] under similarly mild hydro-

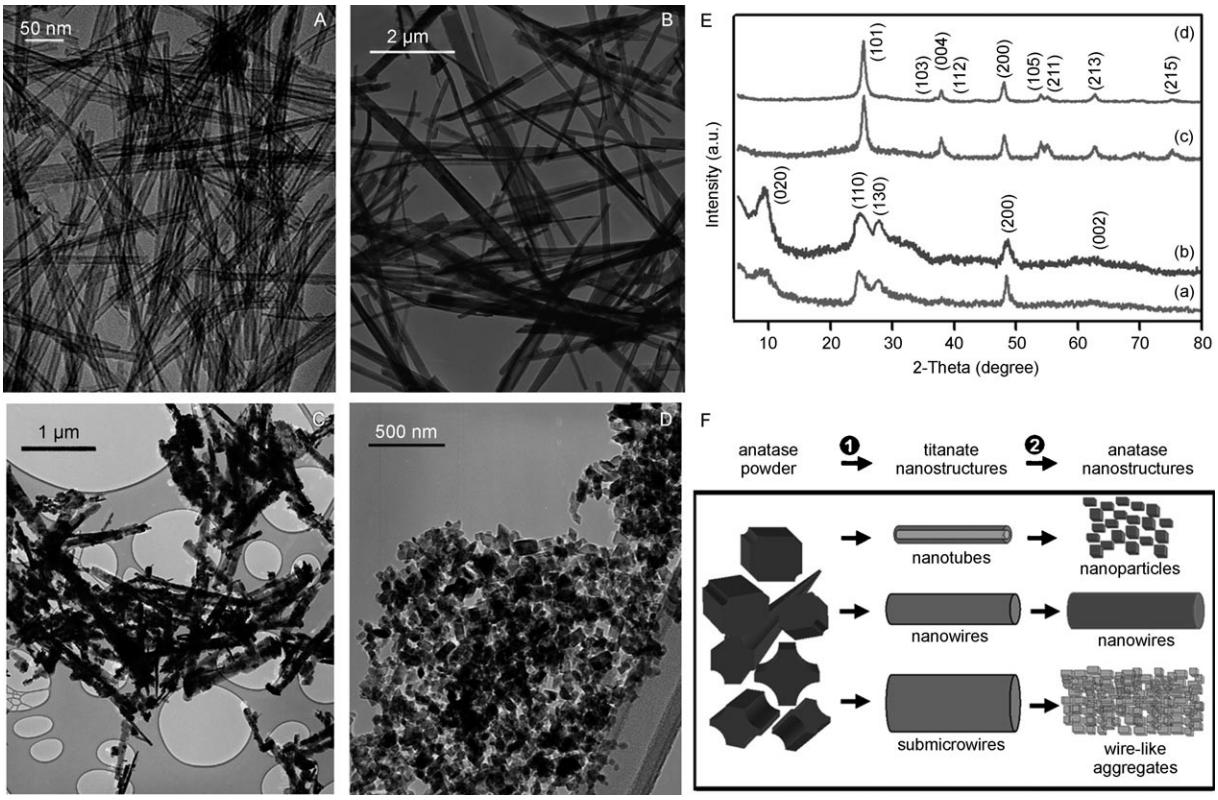

Figure 8. TEM images of as-prepared hydrogen titanate: A) nanotubes, B) nanowires. Corresponding TEM images of as-prepared anatase TiO_2: C) nanowires, D) nanoparticles. E) XRD patterns associated with a) hydrogen titanate nanotubes, b) hydrogen titanate nanowires, c) anatase TiO_2 nanoparticles, d) anatase TiO_2 nanowires. F) Schematic representation of the size- and shape-dependence of the morphological transformation of hydrogen titanate nanostructures into their anatase analogues. Step 1 represents the preparation of hydrogen titanate nanostructures, neutralized from sodium hydrogen titanate nanostructures that, in turn, had been initially hydrothermally synthesized from commercial anatase TiO_2 powder. Step 2 represents the hydrothermal size- and shape-dependent transformation process of orthorhombic protonic lepidocrocite titanate nanostructures into anatase titania nanostructures at 170 °C for 24 h.

small NANO MICRO

thermal conditions. It should be noted that all three of these reactions specifically generating anatase TiO_2 products encompassed an additional hydrothermal processing step involving the initial titanate precursor nanostructures at 170 °C.

This work served as the first report of a controllable size- and shape-dependent morphological change between protonic lepidocrocite titanate and anatase TiO_2 nanostructures, that could readily occur under relatively simple hydrothermal reaction conditions, in neutral solution, and at reasonably low temperatures. Moreover, the as-synthesized crystalline anatase TiO_2 products were single-crystalline and of high purity (without impurities arising from brookite or rutile), all of which are desirable characteristics for nanoparticles with potential applications in photocatalysis and other chemical processes. In fact, these results also indicated that as-synthesized TiO_2 nanostructures possessed noticeably better photocatalytic activity as compared with their commercial counterparts, presumably due to an increase in surface area as well as a rise in crystallinity and reactive surface defect sites.[139,140]

4. Templated Syntheses

Templated syntheses represent a conceptually straightforward approach to the generalized synthesis of nanostructures. In this method, the template simply serves as a structural framework either around or within which another totally distinctive material can be generated in situ and shaped into a nanostructure with its morphology dictated by the size and shape of the template scaffold. The chemical and physical properties of these template membranes (i.e., pore geometry and monodisperse diameters) enable a high degree of control over the dimensions of the resulting 1D nanostructures. Another useful feature of this technique is that it is extremely general with respect to the types of materials that can be prepared. Indeed, nanotubes and nanofibrils of conductive polymers, metals, semiconductors, carbon, and other types of materials have been prepared within the confined cylindrical pores of membranes.[141–145] Moreover, these tubular or fibrillar nanostructures can be assembled into a wide variety of different architectures. For instance, if a nanostructure-containing membrane is attached to a substrate and the membrane were to be removed, an ordered assembly, for example, a vertical array of micro- or nanostructures protruding out from the surface of the substrate, can in principle be obtained.

Many different types of template membranes have been successfully used by various research groups worldwide, and it is generally agreed that templated syntheses are relatively simple, reasonably high-throughput, and cost-effective procedures, all of which are conducive to their generalized applicability and hence, environmental acceptability. There are two general types of templates used – "soft" templates and "hard" templates. Naturally occurring gels, micelles, and chitin scaffolds are considered as soft templates for the precipitation of single crystals of calcium carbonate and of calcium phosphate.[146–148] Other soft templates include DNA strands, polymer matrices, and reverse micelles. Hard templates tend to be associated with materials such as anodic alumina membranes and track-etched polycarbonate membranes, many of which are commercially available.[149]

For the syntheses of complex oxide nanostructures, porous anodic alumina membranes are an ideal choice for templating, because of their high pore density (ranging as high as 10^{11} pores per cm^2), parallel and straight channels, distribution of cylindrical pores of highly uniform diameter arranged in a hexagonal array, and size tunability of $\approx$5 to 300 nm. Moreover, these templates are thermally and mechanically stable.[141–143] However, there is a need to selectively remove these templates without destroying the products, by using either physical and/or chemical post-synthesis treatments in order to collect the desired nanostructures.

As an initial example of demonstrating the viability of template techniques, the first reported synthesis of 1D multiferroic $BiFeO_3$ nanotubes[150] was demonstrated using a pressure-filter variation of a template synthesis involving the sol–gel technique.[151] The generation of $BiFeO_3$ nanotubes is relevant for the design of future nanoscale building blocks for soft magnetic materials with applications in transformers and inductors. $BiFeO_3$ nanotubes, generated from alumina membranes with relatively large pore sizes, mainly consisted of straight and smooth structures with relatively few extraneous particulate debris. These tubes possessed outer diameters in the range of 240 to 300 nm (wall thicknesses of approximately 10 nm), with lengths ranging from a few micrometers to as much as 50 μm, corresponding to the entire length of the template membranes used. In the case of $BiFeO_3$ nanotubes prepared from smaller-diameter pores, the lengths of the nanotubes were not only understandably shorter but also more irregular and polydisperse. Their lengths attained several micrometers at best with diameters in the range of 140 to 180 nm.

In a more recent instance of the practicality of template synthesis, $Bi_2Ti_2O_7$ nanotubes[152] have been synthesized using a sol–gel technique in the presence of an alumina template. $Bi_2Ti_2O_7$ has attracted considerable attention as a useful component of a) gate insulators in advanced metal-oxide semiconductor (MOS) transistors,[153–155] b) storage capacitors in dynamic random access memory (DRAM) applications, and c) buffer layers to improve the electrical properties of ferroelectrics such as $Pb(Zr_{0.5}Ti_{0.5})O_3$ (PZT) and $Bi_4Ti_3O_{12}$.[156–158] The outer diameters of as-prepared bismuth titanate nanotubes ranged from 180 to 330 nm; the wall thickness was approximately 6 nm. The effects of solvent as well as of precursor ratio were also analyzed, with data suggesting a high degree of parameter control over the dimensions and morphology of bismuth titanate nanotubes. Results confirmed the presence of a phase transformation from $Bi_2Ti_2O_7$ to $Bi_4Ti_3O_{12}$ upon increasing annealing temperature. Kinetic studies on the photocatalytic decolorization of methyl orange, with implications for the destruction of environmentally harmful organic contaminants in water, confirmed the higher photocatalytic efficiency of 1D nanoscale motifs of bismuth titanate as compared with the bulk sample.[152]

4.1. $BaCrO_4$, $BaWO_4$

Recently, the conventional template-directed synthesis, popularized by Martin's group,[143,159,160] has been modified and refined to yield a relatively simple and versatile variation with which to prepare size-controlled, one-dimensional nanostructures under extremely mild conditions. This work (Figure 9) demonstrated the room-temperature preparation

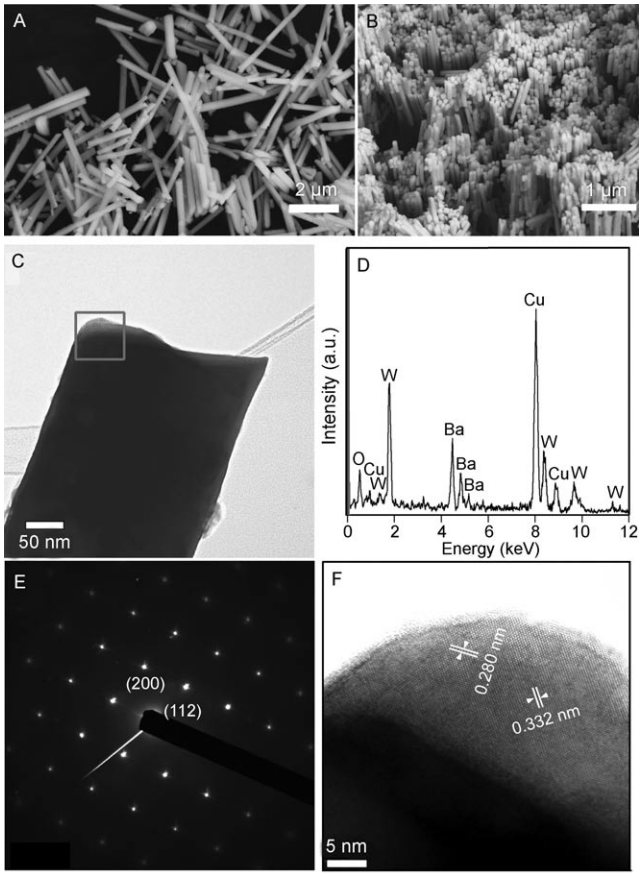

Figure 9. A) Typical SEM micrograph of $BaWO_4$ nanorods. B) SEM image of as-prepared $BaWO_4$ nanorod arrays. C) TEM image of a single $BaWO_4$ nanorod after annealing in air for 5 h at 650 °C. D) EDS of the $BaWO_4$ nanorod shown in (C). Cu peaks originate from the TEM grid. E) SAED pattern and F) high-resolution (HR) TEM image from a portion of the $BaWO_4$ nanorod shown in (C).

of single-crystalline $BaWO_4$ nanorods and $BaCrO_4$ nanorods with different controllable sizes as well as the creation of arrays of these nanorods in the pores of an alumina membrane. Specifically, alumina template membranes with pore sizes of 100 nm and 200 nm were initially hydrated by immersion and sonication in a small volume of distilled, deionized water for a few minutes, so as to avoid air-bubble formation within its structure or on its surface. Subsequently, the membranes were mounted between the two halves of a U-tube cell.[161,162] The half-cells were then filled with equimolar solutions of $Ba(NO_3)_2$ and either Na_2WO_4 or Na_2CrO_4 solutions to generate barium tungstate and chromate, respectively.

In effect, the pores in the alumina membranes were used as the environment in which to control the growth of well-defined morphologies of single crystals of ABO_4 nanostructures. The membranes used were thin, and were mounted in a double-diffusion set-up, which enabled the continuous flow of ions into the membrane pores and thus, the production of single crystals of ABO_4 nanocrystalline materials. After immersion times of up to 12 h at room temperature, the alumina template, into which the precursors had presumably diffused resulting in product formation, was detached and thoroughly washed with deionized water. The alumina membrane was subsequently dissolved by immersion in 1 M NaOH for about 30 min.

What is significant about this protocol is that most nanostructures produced by conventional templating procedures are polycrystalline,[4] in spite of the variety of different deposition strategies used, including electrochemical deposition, electroless deposition, polymerization, sol–gel deposition, and layer-by-layer deposition in nanoporous templates. The reason for the observed polycrystallinity is that many of these standard methodologies require additional post-annealing steps at high temperature (e.g., several hundred degrees Celsius).[141,143,163,164] By contrast, the formation mechanism of nanorods under the ambient experimental conditions used in this study is analogous to a biomimetic crystallization process.[165,166] That is, the growth of ABO_4 nanorods within the confinement of alumina membranes is analogous to the precipitation of single crystals of calcium carbonate[167] (Figure 10) and calcium phosphate within the confinement offered by polymer matrices, gels, micelles, chitin scaffolds, and collagen matrices.[146–148,168] Hence, nucleation and growth of crystalline nanomaterials occur essentially instantaneously through the direct chemical interaction between ions of the two different precursor solutions in contact with each other. The membrane acts to spatially direct crystal growth.

Moreover, at the same time, this simplistic technique allowed for the reproducible fabrication of ordered, monodisperse 3D arrays of these 1D nanomaterials. This is critical, because assembly of nanoscale components (here nanorods) is a key step towards building functional devices,[169] important for applications including nanoscale electronics and molecular sensing. Specifically, the fabrication of 3D arrays of 1D nanomaterials, such as nanorods, is useful for optoelectronic applications, such as room-temperature ultraviolet lasing.[170] Furthermore, although the primary focus of the initial work was on isolated 100- and 200-nm-sized $BaWO_4$ and $BaCrO_4$ nanorods and their associated arrays (Figure 9), it was noted that different sizes of these various nanoscale architectures[171,172] could be reproducibly formed using alumina template membranes of varying pore sizes.

4.2. CaF_2, BaF_2, SrF_2

Fluorides have wide applications in optics, as windows, biological labels, and lenses,[173–175] as well as components of insulators, gate dielectrics, wide-gap insulating overlayers, and buffer layers in semiconductor-on-insulator struc-

small NANO MICRO

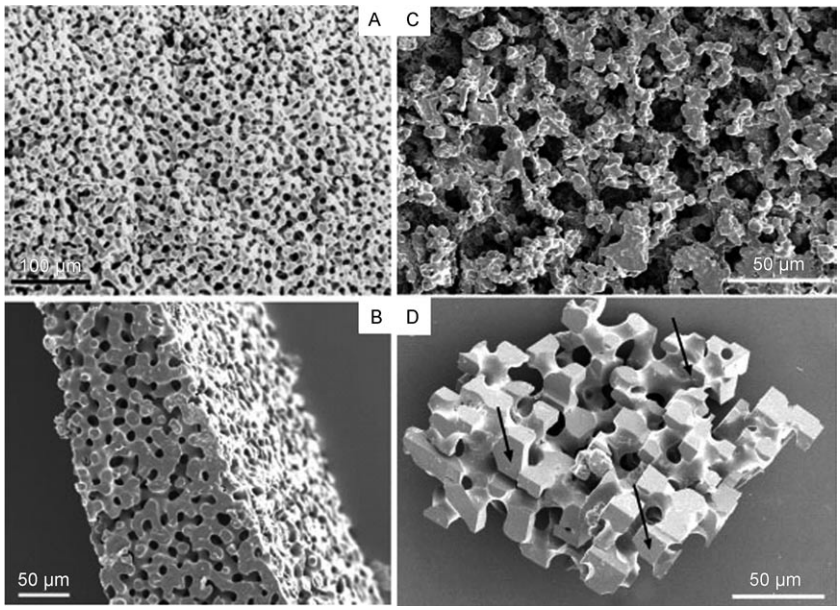

Figure 10. A) Cross section through a sea urchin skeletal plate, showing a spongelike structure. B) Polymer replica of a sea urchin plate; calcium carbonate precipitated in the polymer membrane. C) Polycrystalline particles templated from 0.4 M solutions of reagents. D) Templated single crystal of calcite precipitated from 0.02 M solutions of calcium chloride and sodium carbonate. The arrows in (D) refer to the rhombohedral geometry of the faces at the termini of the crystals, uniquely associated with the calcite polymorph of $CaCO_3$. Moreover, these data indicate that faces on different termini are aligned and that the entire particle is likely to be a single crystal, in spite of its complex morphology. Adapted from Ref. [167].

tures.[176] In addition, fluorides doped with rare-earth ions such as Eu^{3+}, Nd^{3+}, and Ho^{3+} have also been reported to display unique luminescence properties with correspondingly useful applications in diagnostics, lasing, solid-state light emitters, light amplification, optical telecommunication, and upconversion.[177–179] Hence, it is reasonable to expect that nanoscale fluorides will play an important role in technological applications including high-density optical storage devices, nanosensors, and color displays.[180–182]

The key synergistic advance, enabling and fostering the success of this reaction, was to substitute the use of anodic alumina membranes in these templating techniques with other classes of membranes, including track-etch polycarbonate membranes. This was an important technical issue to resolve, because the etching reagent for alumina membranes, NaOH, will react readily with nanoscale fluoride products, whereas polycarbonate membranes can be removed through simple dissolution with a noninterfering, organic solvent such as dichloromethane.[183–185]

All of the data (Figure 11) collected suggest that as-prepared alkaline-earth-metal fluoride nanowires are monodisperse with controllable morphology. In other words, the ambient synthesis of straight, crystalline wirelike structures is possible using a modified template-directed method without the need for either sophisticated experimental setups or high-temperature annealing. Moreover, the shapes and sizes of these fluoride nanowires accurately replicated the interior pore structure as well as the pore lengths and diameters of the polycarbonate templates from whence they were generated. Furthermore, as a demonstration of principle, as-prepared alkaline-earth-metal fluoride nanowire samples, doped with either Eu^{3+} or Tb^{3+} ions, displayed either pink or green luminescence, respectively, under UV-lamp excitation.

5. Summary and Outlook

The environmentally acceptable protocols we have focused on in this work include 1) molten-salt synthesis protocols, 2) solvothermal/hydrothermal methods, and finally 3) template-directed techniques.

The green advantages of the MSS protocol are that it is simplistic, is readily scaleable, and uses relatively nontoxic reaction media and reagents (e.g., table salt). Applications of this method to the synthesis of $SrTiO_3$ nanocubes, $BaTiO_3$, $Ca_{1-x}Sr_xTiO_3$, and $BaZrO_3$ nanoparticles, $Bi_2Fe_4O_9$ submicrometer cubes, as well as hematite and iron/magnetite nanocomposites have been extensively discussed.

The environmentally acceptable attributes of solvothermal/hydrothermal methods are that a) they are relatively large scale and high yield in terms of the quantity of desired products generated without substantial amounts of harmful byproducts, b) they can frequently use water as the solvent medium, and c) they can be run at reasonably low temperatures using cost-efficient, experimentally facile protocols. It is fortunate that variations of this methodology have been successfully applied to the synthesis of $BaTiO_3$ and $SrTiO_3$ nanotubes as well as to titanate and titania 0D, 1D, and 3D nanostructures.

Finally, what is fundamentally environmentally progressive about the modified template techniques described is the fact these reactions can be run under ambient conditions in aqueous solution with reliable control over shape, dimensionality, and crystallinity. The potential is to generalize this protocol to the synthesis of not only isolated structures but also arrays of different classes of materials including ternary metal oxides. The validity of these techniques has been demonstrated in the synthesis of $BaWO_4$ and $BaCrO_4$ nanorods, of arrays of $BaWO_4$ and $BaCrO_4$ nanorods, and of fluoride nanowires.

Our group has long-standing goals of creating well-defined nanoscale building blocks with tailorable properties. We have been interested in relatively simple synthesis methods whose ideal attributes include stability as well as control of size, shape, morphology, and chemical composition in the

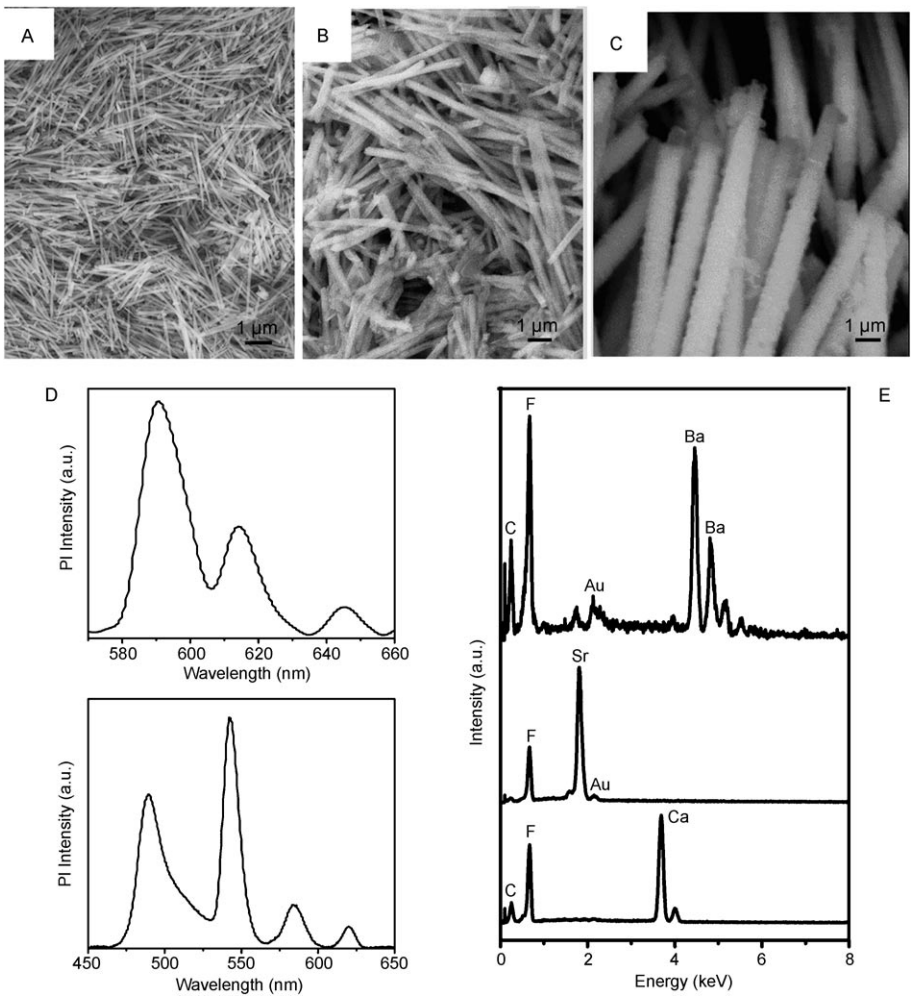

Figure 11. Typical SEM images of A) CaF_2 nanowires prepared using polycarbonate membranes with 50 nm pore sizes, B) SrF_2 nanowires prepared using polycarbonate membranes with 100 nm pore diameters, and C) BaF_2 nanowires generated using polycarbonate membranes with pores measuring 200 nm. D) Photoluminescence spectra of as-prepared CaF_2 nanowires doped with Eu^{3+} (top) and Tb^{3+} ions (bottom). E) EDS data of as-synthesized alkaline-earth-metal fluoride nanowires, corresponding to the SEM images shown in (A–C): CaF_2 (bottom), SrF_2 (middle), and BaF_2 (top). The C and Au peaks originate from the conductive carbon tape and gold coating, respectively.

ultimate product. It is evident that the cost-effective techniques we have described herein are a step in the right direction towards developing processes that allow for minimal impact (i.e., relatively benign reagents; little waste generation[186]) on the environment without sacrificing on sample quality and quantity. Of course, all of these methods require constant optimization as well as real-time, in-process monitoring. In the latter context, time-resolved in situ high-temperature X-ray diffraction has been used recently to probe the kinetics and mechanism of a molten-salt synthesis route towards the production of mixed-valence sodium titanate, suggesting that the reaction occurred at the surfaces of the solid particles mediated by the molten-salt flux.[187]

We have not had the opportunity to analyze a number of other environmentally significant, conceptually exciting techniques reported in nanomaterials synthesis by other laboratories. One of the more interesting methods includes the use of biomimetic chemistry to generate nanomaterials. For biomimetic chemistry,[188–190] the approach involves the utilization of actual biomolecular entities such as proteins, bacteria, and viruses to act either as a growth medium or as a spatially constrained nanoscale reactor for the generation of metal oxide nanoparticles; one interesting example of the latter is the synthesis of paratungstate and decavanadate particles encapsulated within the protein cages of viruses. Moreover, as an illustration of the potential of iron-oxidizing bacteria, ferrihydrite particles have been found to self-assemble on *Gallionella* stalks to form colloidal aggregates.

In addition, many other protocols are still being developed that attempt to use ever fewer and ever safer, air-stable reagents and solvents under relatively low temperature conditions. One of the most notable efforts in this regard has been the push towards generating high-quality semiconductor nanocrystals[191] with well-controlled size and shape distributions using low-cost, safe raw materials (e.g., the use of cadmium acetate[192] as a precursor as opposed to dimethylcadmium; the utilization of starch as a capping agent[193]) without the need for a glove box. A specific modification[194] of this experiment using cadmium oxide as a precursor can be run at 225 °C for 1 h, yielding CdSe nanoparticles ranging from 1.8 to 4 nm in diameter. Another area of interest has been the development of surface-functionalized nanostructures using green techniques; the processing[195] of organic-capped anatase TiO_2 nanorods by the hydrolysis of titanium tetraisopropoxide in oleic acid surfactant at 80 °C comes to mind in this context.

It is evident that with all of the fabrication techniques described herein that the novel modifications and improvements that render these methods more efficient and less environmentally harmful are constantly being reported in the literature. One can only hope for the widespread dissemination as well as for the universal adoption of this growing and increasingly significant trend in synthetic nanochemistry.

Acknowledgements

Research was supported in part by the U.S. Department of Energy Office of Basic Energy Sciences under Contract DE-AC02-98CH10886 for personnel support and equipment usage. Acknowledgement is also made to the National Science Foundation (CAREER award DMR-0348239), and the Alfred P. Sloan Foundation (2006–2008) for PI support of this research.

[1] J. Hu, T. W. Odom, C. M. Lieber, *Acc. Chem. Res.* **1999**, *32*, 435.
[2] G. R. Patzke, F. Krumeich, R. Nesper, *Angew. Chem.* **2002**, *114*, 2554; *Angew. Chem. Int. Ed.* **2002**, *41*, 2446.
[3] C. N. R. Rao, M. Nath, *Dalton Trans.* **2003**, 1.
[4] Y. Xia, P. Yang, Y. Sun, Y. Wu, B. Mayers, B. Gates, Y. Yin, F. Kim, H. Yan, *Adv. Mater.* **2003**, *15*, 353.
[5] M. A. El-Sayed, *Acc. Chem. Res.* **2004**, *37*, 326.
[6] S. Sun, C. B. Murray, D. Weller, L. Folks, A. Moser, *Science* **2000**, *287*, 1989.
[7] X. Wang, Y. Li, *Pure Appl. Chem.* **2006**, *78*, 45.
[8] L. L. Sohn, *Nature* **1998**, *394*, 131.
[9] M. S. Dresselhaus, G. Dresselhaus, P. Avouris, *Carbon Nanotubes: Synthesis Structure, Properties, and Applications*, Springer Verlag, Berlin **2001**.
[10] A. P. Alivisatos, *J. Phys. Chem.* **1996**, *100*, 13226.
[11] R. H. Baughman, A. A. Zakhidov, W. A. de Heer, *Science* **2002**, *297*, 787.
[12] M. Bruchez, M. Moronne, P. Gin, S. Weiss, A. P. Alivisatos, *Science* **1998**, *281*, 2013.
[13] W. U. Huynh, J. J. Dittmer, A. P. Alivisatos, *Science* **2002**, *295*, 2425.
[14] V. Lordi, N. Yao, J. Wei, *Chem. Mater.* **2001**, *13*, 733.
[15] J. E. Fischer, H. Dai, A. Thess, R. Lee, N. M. Hanjani, D. L. Dehaas, R. E. Smalley, *Phys. Rev. B* **1997**, *55*, R4921.
[16] K. S. Shankar, A. K. Raychaudhuri, *Mater. Sci. Eng., C* **2005**, *25*, 738.
[17] P. Raveendran, J. Fu, S. L. Wallen, *Green Chem.* **2006**, *8*, 34.
[18] L. C. McKenzie, J. E. Hutchison, *Chemistry Today* **2004**, *22*, 30.
[19] R. E. Cable, R. E. Schaak, *Chem. Mater.* **2005**, *17*, 6835.
[20] R. E. Schaak, T. E. Mallouk, *Chem. Mater.* **2002**, *14*, 1455.
[21] N. R. Jana, X. Peng, *J. Am. Chem. Soc.* **2003**, *125*, 14280.
[22] C. J. Murphy, T. K. Sau, A. M. Gole, C. J. Orendorff, J. Gao, L. Gou, S. E. Hunyadi, T. Li, *J. Phys. Chem. B* **2005**, *109*, 13857.
[23] R. E. Schaak, A. K. Sra, B. M. Leonard, R. E. Cable, J. C. Bauer, Y.-F. Han, J. Means, W. Teizer, Y. Vasquez, E. S. Funck, *J. Am. Chem. Soc.* **2005**, *127*, 3506.
[24] W. W. Weare, S. M. Reed, M. G. Warner, J. E. Hutchison, *J. Am. Chem. Soc.* **2000**, *122*, 12890.
[25] P. T. Anastas, M. M. Kirchhoff, *Acc. Chem. Res.* **2002**, *35*, 686.
[26] Y. Yang, K. M. Saoud, V. Abdelsayed, G. Glaspell, S. Deevi, M. S. El-Shall, *Catal. Commun.* **2006**, *7*, 281.
[27] B. L. Abrams, J. P. Wilcoxon, *Crit. Rev. Solid State Mater. Sci.* **2005**, *30*, 153.
[28] I. Kiricsi, A. Molnar, I. Palinko, A. Fudala, J. B. Nagy, *Solid State Ionics* **1997**, *101*, 793.
[29] V. R. Choudhary, A. Dhar, P. Jana, R. Jha, B. S. Uphade, *Green Chem.* **2005**, *7*, 768.
[30] V. Mevellec, A. Roucoux, *Inorg. Chim. Acta* **2004**, *357*, 3099.
[31] B.-Z. Zhan, M. A. White, T.-K. Sham, J. A. Pincock, R. J. Doucet, K. V. R. Rao, K. N. Robertson, T. S. Cameron, *J. Am. Chem. Soc.* **2003**, *125*, 2195.
[32] T. Kashiwagi, F. Du, J. F. Douglas, K. I. Winey, R. H. Harris Jr. , J. R. Shields, *Nat. Mater.* **2005**, *4*, 928.
[33] N. Savage, M. S. Diallo, *J. Nanopart. Res.* **2005**, *7*, 331.
[34] R. Tartivel, E. Reynaud, F. Grasset, J.-C. Sangleboeuf, T. Rouxel, *J. Non-Cryst. Solids* **2007**, *353*, 108.
[35] Y. Hayashi, T. Kimura, T. Yamaguchi, *J. Mater. Sci.* **1986**, *21*, 757.
[36] R. Zboril, M. Mashlan, D. Petridis, *Chem. Mater.* **2002**, *14*, 969.
[37] K. H. Yoon, Y. S. Cho, D. H. Kang, *J. Mater. Sci.* **1998**, *33*, 2977.
[38] M. Wilbert, R. Rothe, K. Landfester, M. Antonietti, *Chem. Mater.* **2001**, *13*, 4681.
[39] W. Wang, Y. Zhan, Y. Wang, X. Wang, Y. Liu, C. Zheng, G. Wang, *Mater. Res. Bull.* **2002**, *37*, 1093.
[40] Y. Wang, J. Y. Lee, *J. Phys. Chem. B* **2004**, *108*, 17832.
[41] W. Wang, C. Xu, G. Wang, Y. Liu, C. Zheng, *Adv. Mater.* **2002**, *14*, 837.
[42] Y. Liu, C. Zheng, W. Wang, C. Yin, G. Wang, *Adv. Mater.* **2001**, *13*, 1883.
[43] C. Xu, X. Zhao, S. Liu, G. Wang, *Solid State Commun.* **2003**, *125*, 301.
[44] Z. Yang, Y. Gu, L. Chen, L. Shi, J. Ma, Y. Qian, *Solid State Commun.* **2004**, *130*, 347.
[45] H. Liu, C. Hu, Z. L. Wang, *Nano Lett.* **2006**, *6*, 1535.
[46] W. Wang, B. Zeng, J. Yang, B. Poudel, J. Huang, M. J. Naughton, Z. Ren, *Adv. Mater.* **2006**, *18*, 3275.
[47] Y. Tian, D. Chen, X. Jiao, *Chem. Mater.* **2006**, *18*, 6088.
[48] N. A. Hill, *J. Phys. Chem. B* **2000**, *104*, 6694.
[49] J. F. Scott, *Ferroelectr. Rev.* **1998**, *1*, 1.
[50] A. J. Millis, *Nature* **1998**, *392*, 147.
[51] T. K. Song, J. Kim, S.-I. Kwun, *Solid State Commun.* **1996**, *97*, 143.
[52] L. A. Willis, W. Wessels, D. S. Richeson, T. J. Marks, *Appl. Phys. Lett.* **1992**, *60*, 41.
[53] J. Zhang, C. P. J. Beetz, S. B. Krupanidhi, *Appl. Phys. Lett.* **1994**, *65*, 2410.
[54] J. Zhao, V. Fuflygin, F. Wang, P. E. Norris, L. Bouthilette, C. Woods, *J. Mater. Chem.* **1997**, *7*, 933.
[55] L. Z. Wang, S. J. Tomura, F. Ohashi, M. Maeda, M. Suzuki, K. Inukai, *J. Mater. Chem.* **2001**, *11*, 1465.
[56] Y. Mao, S. Banerjee, S. S. Wong, *J. Am. Chem. Soc.* **2003**, *125*, 15718.
[57] Y.-J. Chen, J.-B. Li, Q.-M. Wei, H.-Z. Zhai, *J. Cryst. Growth* **2001**, *224*, 244.
[58] Y. Sun, Y. Xia, *Science* **2002**, *298*, 2176.
[59] T. S. Ahmadi, Z. L. Wang, T. C. Green, A. Henglein, M. A. El-Sayed, *Science* **1996**, *272*, 1924.
[60] Z. L. Wang, *J. Phys. Chem. B* **2000**, *104*, 1153.
[61] R. Ranjan, D. Pandrey, *J. Phys. Condens. Matter* **1999**, *11*, 2247.
[62] S. Qin, A. I. Becerro, F. Seifert, J. Gottsmann, J. Jiang, *J. Mater. Chem.* **2000**, *10*, 1609.
[63] J. L. Ribeiro, M. T. Lacerda-Aroso, M. R. Chaves, M. Maglione, A. Almeida, *J. Phys. Condens. Matter* **1999**, *11*, 1247.
[64] T. Mistui, W. B. Westphal, *Phys. Rev.* **1961**, *124*, 1354.
[65] C. J. Ball, B. D. Begg, D. J. Cookson, G. J. Thorogood, E. R. Vance, *J. Solid State Chem.* **1998**, *139*, 238.
[66] R. Ranjan, D. Pandey, W. Schuddinck, O. Richard, P. De Meulenaere, J. Van Landuyt, G. Van Tendeloo, *J. Solid State Chem.* **2001**, *162*, 20.
[67] R. Li, Q. Tang, S. Yin, Y. Yamaguchi, T. Sato, *Chem. Lett.* **2004**, *33*, 412.
[68] R. Ranjan, D. Pandey, N. P. Lalla, *Phys. Rev. Lett.* **2000**, *84*, 3726.
[69] Y. Mao, S. S. Wong, *Adv. Mater.* **2005**, *17*, 2194.
[70] S. Banerjee, D.-I. Kim, R. D. Robinson, I. P. Herman, Y. Mao, S. S. Wong, *Appl. Phys. Lett.* **2006**, *89*, 223130.
[71] H. Zhou, Y. Mao, S. S. Wong, *J. Mater. Chem.* **2007**, *17*, 1707.
[72] W. E. Buhro, V. L. Colvin, *Nat. Mater.* **2003**, *2*, 138.

[73] X. Peng, L. Manna, P. Yang, J. Wickham, E. Scher, A. Kadavanich, A. P. Alivisatos, *Nature* **2000**, *404*, 59.
[74] T.-J. Park, S. S. Wong, *Chem. Mater.* **2006**, *18*, 5289.
[75] T. Hyeon, *Chem. Commun.* **2003**, 927.
[76] J. Chen, L. Xu, W. Li, X. Gou, *Adv. Mater.* **2005**, *17*, 582.
[77] M. A. Gondal, A. Hameed, Z. H. Yamani, A. Suwaiyan, *Chem. Phys. Lett.* **2004**, *385*, 111.
[78] T. Ohmori, H. Takahashi, H. Mametsuka, E. Suzuki, *Phys. Chem. Chem. Phys.* **2000**, *2*, 3519.
[79] F. J. Morin, *Phys. Rev. B: Solid State* **1950**, *78*, 819.
[80] E. J. W. Verwey, *Nature* **1939**, *144*, 327.
[81] H. Deng, X. Li, Q. Peng, X. Wang, J. Chen, Y. Li, *Angew. Chem.* **2005**, *117*, 2842; *Angew. Chem. Int. Ed.* **2005**, *44*, 2782.
[82] N. I. Zakharchenko, *Kinet. Catal.* **2002**, *43*, 95.
[83] Y. Xiong, M. Wu, Z. Peng, N. Jiang, Q. Chen, *Chem. Lett.* **2004**, *33*, 502.
[84] T.-J. Park, G. C. Papaefthymiou, A. R. Moodenbaugh, Y. Mao, S. S. Wong, *J. Mater. Chem.* **2005**, *15*, 2099.
[85] A. G. Tutov, I. E. Myl'nikova, N. N. Parfenova, V. A. Bokov, S. A. Kizhaev, *Sov. Phys. Solid State* **1964**, *6*, 963.
[86] M. Rajamathi, R. Seshadri, *Curr. Opin. Solid State Mater. Sci.* **2002**, *6*, 337.
[87] C. Burda, X. Chen, R. Narayanan, M. A. El-Sayed, *Chem. Rev.* **2005**, *105*, 1025.
[88] K. Byrappa, M. Yoshimura, *Handbook of Hydrothermal Technology*, William Andrew Publishing, LLC, New York **2001**.
[89] A. Michailovski, G. R. Patzke, *Chem. Eur. J.* **2006**, *12*, 9122.
[90] B. Jancar, D. Suvorov, *Nanotechnology* **2006**, *17*, 25.
[91] P. Gao, Y. Xie, Y. Chen, L. Ye, Q. Guo, *J. Cryst. Growth* **2005**, *285*, 555.
[92] H.-S. Qian, S.-H. Yu, J.-Y. Gong, L.-B. Luo, L.-F. Fei, *Langmuir* **2006**, *22*, 3830.
[93] S.-B. Wang, Y.-L. Min, S.-H. Yu, *J. Phys. Chem. C* **2007**, *111*, 3551.
[94] B. L. Cushing, V. L. Kolesnichenko, C. J. O'Connor, *Chem. Rev.* **2004**, *104*, 3893.
[95] P. Gao, Y. Xie, L. Ye, Y. Chen, Z. Li, *Chem. Lett.* **2006**, *35*, 162.
[96] X. Cui, S.-H. Yu, L. Li, B. Liu, H. Li, M. Mo, X.-M. Liu, *Chem. Eur. J.* **2004**, *10*, 218.
[97] Y. Xiong, Z. Li, R. Zhang, Y. Xie, J. Yang, C. Wu, *J. Phys. Chem. B* **2003**, *107*, 3697.
[98] X. Wang, Y. Li, *Angew. Chem.* **2002**, *114*, 4984; *Angew. Chem. Int. Ed.* **2002**, *41*, 4790.
[99] Y. Li, J. Wang, Z. Deng, Y. Wu, X. Sun, D. Yu, P. Yang, *J. Am. Chem. Soc.* **2001**, *123*, 9904.
[100] X. Wang, X. Sun, D. Yu, B. Zou, Y. Li, *Adv. Mater.* **2003**, *15*, 1442.
[101] G. R. Patzke, A. Michailovski, F. Krumeich, R. Nesper, J. D. Grunwaldt, A. Baiker, *Chem. Mater.* **2004**, *16*, 1126.
[102] A. Michailovski, F. Krumeich, G. R. Patzke, *Chem. Mater.* **2004**, *16*, 1433.
[103] A. Michailovski, F. Krumeich, G. R. Patzke, *Helv. Chim. Acta* **2004**, *87*, 1029.
[104] X. Wang, Y. Li, *Inorg. Chem.* **2006**, *45*, 7522.
[105] J. Wang, Y. Li, *Adv. Mater.* **2003**, *15*, 445.
[106] B. Li, Y. Xu, G. Rong, M. Jing, Y. Xie, *Nanotechnology* **2006**, *17*, 2560.
[107] X. Sun, J. Liu, Y. Li, *Chem. Mater.* **2006**, *18*, 3486.
[108] H.-S. Qian, S.-H. Yu, J.-Y. Gong, L.-B. Luo, L.-L. Wen, *Cryst. Growth Des.* **2005**, *5*, 935.
[109] J. F. Bertone, J. Cizeron, R. Wahi, J. K. Bosworth, V. L. Colvin, *Nano Lett.* **2003**, *3*, 655.
[110] A. Cabanas, J. A. Darr, E. Lester, M. Poliakoff, *Chem. Commun.* **2000**, 901.
[111] F. Gao, Q. Ku, S. Komarneni, *J. Nanosci. Nanotechnol.* **2006**, *6*, 3812.
[112] S. Komarneni, R. Roy, Q. H. Li, *Mater. Res. Bull.* **1992**, *27*, 1393.
[113] M. M. Lencka, R. E. Riman, *Chem. Mater.* **1993**, *5*, 61.
[114] C. T. Xia, E. W. Shi, W. Z. Zhong, J. K. Guo, *J. Cryst. Growth* **1996**, *166*, 961.
[115] J. O. Eckert Jr. , C. C. Hung-Houston, B. L. Gersten, M. M. Lencka, R. E. Roman, *J. Am. Ceram. Soc.* **1996**, *79*, 2929.
[116] I. J. Clark, T. Takeuchi, N. Ohtori, D. C. Sinclair, *J. Mater. Chem.* **1999**, *9*, 83.
[117] P. K. Dutta, J. R. Gregg, *Chem. Mater.* **1992**, *4*, 843.
[118] P. K. Dutta, R. Asiaie, S. A. Akbar, W. D. Zhu, *Chem. Mater.* **1994**, *6*, 1542.
[119] M. Z.-C. Hu, V. Kurian, E. A. Payzant, C. J. Rawn, R. D. Hunt, *Powder Technol.* **2000**, *110*, 2.
[120] T. Kasuga, M. Hiramatsu, A. Hosen, T. Sekino, K. Niihara, *Langmuir* **1998**, *14*, 3160.
[121] T. Kasuga, M. Hiramatsu, A. Hoson, T. Sekino, K. Niihara, *Adv. Mater.* **1999**, *11*, 1307.
[122] Y. Mao, S. Banerjee, S. S. Wong, *Chem. Commun.* **2003**, 408.
[123] Q. Wang, Q. Gao, J. Shi, *J. Am. Chem. Soc.* **2004**, *126*, 14346.
[124] N. Masaki, S. Uchida, H. Yamane, T. Sato, *Chem. Mater.* **2002**, *14*, 419.
[125] M. Grätzel, *Nature* **2001**, *414*, 318.
[126] M. R. Hoffmann, S. T. Martin, W. Choi, D. W. Bahnemann, *Chem. Rev.* **1995**, *95*, 69.
[127] O. K. Varghese, D. Gong, M. Paulose, K. G. Ong, E. C. Dickey, C. A. Grimes, *Adv. Mater.* **2003**, *15*, 624.
[128] C. Xu, Y. Zhan, K. Hong, G. Wang, *Solid State Commun.* **2003**, *126*, 545.
[129] D. V. Bavykin, V. N. Parmon, A. A. Lapkin, F. C. Walsh, *J. Mater. Chem.* **2004**, *14*, 3370.
[130] M. Hodos, E. Horváth, H. Haspel, Á. Kukovecz, Z. Kónya, I. Kiricsi, *Chem. Phys. Lett.* **2004**, *399*, 512.
[131] H. Y. Zhu, Y. Lan, X. P. Gao, S. P. Ringer, Z. F. Zheng, D. Y. Song, J. C. Zhao, *J. Am. Chem. Soc.* **2005**, *127*, 6730.
[132] C. Wu, Y. Xie, D. Wang, J. Yang, T. Li, *J. Phys. Chem. B* **2003**, *107*, 13583.
[133] F. Caruso, X. Shi, R. A. Caruso, A. Susha, *Adv. Mater.* **2001**, *13*, 740.
[134] Y. Mao, M. Kanungo, T. Hemraj-Benny, S. S. Wong, *J. Phys. Chem. B* **2006**, *110*, 702.
[135] H. Zhu, X. Gao, Y. Lan, D. Song, Y. Xi, J. Zhao, *J. Am. Chem. Soc.* **2004**, *126*, 8380.
[136] Q. Feng, M. Hirasawa, K. Yanagisawa, *Chem. Mater.* **2001**, *13*, 290.
[137] Y. Mao, S. S. Wong, *J. Am. Chem. Soc.* **2006**, *128*, 8217.
[138] B. Liu, S.-H. Yu, L. Li, F. Zhang, Q. Zhang, M. Yoshimura, P. Shen, *J. Phys. Chem. B* **2004**, *108*, 2788.
[139] Y. Xu, C. H. Langford, *Langmuir* **2001**, *17*, 897.
[140] H. D. Jang, S.-K. Kim, S.-J. Kim, *J. Nanopart. Res.* **2001**, *3*, 141.
[141] G. Schmid, *J. Mater. Chem.* **2002**, *12*, 1231.
[142] T. E. Mallouk, *Science* **2001**, *291*, 443.
[143] J. C. Hulteen, C. R. Martin, *J. Mater. Chem.* **1997**, *7*, 1075.
[144] N. I. Kovtyukhova, T. E. Mallouk, T. S. Mayer, *Adv. Mater.* **2003**, *15*, 780.
[145] N. I. Kovtyukhova, B. K. Kelly, T. E. Mallouk, *J. Am. Chem. Soc.* **2004**, *126*, 12738.
[146] A. Becker, W. Becker, J. C. Marxen, M. Epple, *Z. Anorg. Allg. Chem.* **2003**, *629*, 2305.
[147] O. Grassmann, P. Lobmann, *Biomaterials* **2004**, *25*, 277.
[148] K. Schwarz, M. Epple, *Chem. Eur. J.* **1998**, *4*, 1898.
[149] Q. Lu, F. Gao, S. Komarneni, T. E. Mallouk, *J. Am. Chem. Soc.* **2004**, *126*, 8650.
[150] T.-J. Park, Y. Mao, S. S. Wong, *Chem. Commun.* **2004**, 2708.
[151] M. Steinhart, J. H. Wendorff, A. Greiner, R. B. Wehrspohn, K. Nielsch, J. Schilling, J. Choi, U. Gösele, *Science* **2002**, *296*, 1997.

[152] H. Zhou, T.-J. Park, S. S. Wong, *J. Mater. Res.* **2006**, *21*, 2941.
[153] G. W. Hwang, W. D. Kim, Y.-S. Min, Y. J. Cho, C. S. Hwang, *J. Electrochem. Soc.* **2006**, *153*, F20.
[154] X. N. Yang, B. B. Huang, H. B. Wang, S. X. Shang, W. F. Yao, J. Y. Wei, *J. Cryst. Growth* **2004**, *270*, 98.
[155] S. W. Wang, H. Wang, X. Wu, S. Shang, M. Wang, Z. Li, W. Lu, *J. Cryst. Growth* **2001**, *224*, 323.
[156] X. Wu, S. W. Wang, H. Wang, Z. Wang, S. X. Shang, M. Wang, *Thin Solid Films* **2000**, *370*, 30.
[157] S. W. Wang, H. Wang, S. X. Shang, J. Huang, Z. Wang, M. Wang, *J. Cryst. Growth* **2000**, *217*, 388.
[158] W. Wu, K. Fumoto, Y. Oishi, M. Okuyama, Y. Hamakawa, *Jpn. J. Appl. Phys., Part 1* **1996**, *35*, 1560.
[159] C. R. Martin, *Science* **1994**, *266*, 1961.
[160] C. R. Martin, *Chem. Mater.* **1996**, *8*, 1739.
[161] C. R. Martin, L. S. Van Dyke, Z. Cai, W. Liang, *J. Am. Chem. Soc.* **1990**, *112*, 8976.
[162] W. Liang, C. R. Martin, *Chem. Mater.* **1991**, *3*, 390.
[163] B. B. Lakshmi, P. K. Dorhout, C. R. Martin, *Chem. Mater.* **1997**, *9*, 857.
[164] S. J. Limmer, S. Seraji, Y. Wu, T. P. Chou, C. Nguyen, G. Cao, *Adv. Funct. Mater.* **2002**, *12*, 59.
[165] S. V. Dorozhkin, E. I. Dorozhkina, M. Epple, *Cryst. Growth Des.* **2004**, *4*, 389.
[166] E. Loste, R. J. Park, J. Warren, F. C. Meldrum, *Adv. Funct. Mater.* **2004**, *14*, 1211.
[167] R. J. Park, F. C. Meldrum, *Adv. Mater.* **2002**, *14*, 1167.
[168] G. Falini, S. Fermani, A. Ripamonti, *J. Inorg. Biochem.* **2002**, *91*, 475.
[169] H. Cölfen, S. Mann, *Angew. Chem.* **2003**, *115*, 2452; *Angew. Chem. Int. Ed.* **2003**, *42*, 2350.
[170] M. H. Huang, S. Mao, H. Feick, H. Yan, Y. Wu, H. Kind, E. Weber, R. Russo, P. Yang, *Science* **2001**, *292*, 1897.
[171] P. Yang, *Nature* **2003**, *425*, 243.
[172] Z. R. Tian, J. A. Voigt, J. Liu, B. McKenzie, M. J. Mcdermott, M. A. Rodriguez, H. Konishi, H. Xu, *Nat. Mater.* **2003**, *2*, 821.
[173] C. M. Bender, J. M. Burlitch, D. Barber, C. Pollock, *Chem. Mater.* **2000**, *12*, 1969.
[174] H. Lian, J. Liu, Z. Ye, C. Shi, *Chem. Phys. Lett.* **2004**, *386*, 291.
[175] R. Hua, C. Zang, C. Shao, D. Xie, C. Shi, *Nanotechnology* **2003**, *14*, 588.
[176] R. Singh, S. Sinha, P. Chou, N. J. Hsu, F. Radpour, *J. Appl. Phys.* **1989**, *66*, 6179.
[177] L. F. Johnson, H. J. Guggenheim, *Appl. Phys. Lett.* **1971**, *19*, 44.
[178] X. X. Zhang, P. Hong, M. Bass, B. H. T. Chai, *Phys. Rev. B* **1995**, *51*, 9298.
[179] P. Xie, S. C. Rand, *Opt. Lett.* **1992**, *17*, 1198.
[180] M. Cao, C. Hu, E. Wang, *J. Am. Chem. Soc.* **2003**, *125*, 11196.
[181] M. Cao, Y. Wang, Y. Qi, C. Guo, C. Hu, *J. Solid State Chem.* **2004**, *177*, 2205.
[182] G. De, W. Qin, J. Zhang, D. Zhao, J. Zhang, *Chem. Lett.* **2005**, *34*, 914.
[183] L. Suber, P. Imperatori, G. Ausanio, F. Fabbri, H. Hofmeister, *J. Phys. Chem. B* **2005**, *109*, 7103.
[184] C. Schönenberger, B. M. I. van der Zande, L. G. J. Fokkink, M. Henny, C. Schmid, M. Kruger, A. Bachtold, R. Huber, H. Birk, U. Staufer, *J. Phys. Chem. B* **1997**, *101*, 5497.
[185] P. Porrata, E. Goun, H. Matsui, *Chem. Mater.* **2002**, *14*, 4378.
[186] M. Poliakoff, J. M. Fitzpatrick, T. R. Farren, P. T. Anastas, *Science* **2002**, *297*, 807.
[187] M. J. Geselbracht, L. D. Noailles, L. T. Ngo, J. H. Pikul, R. I. Walton, E. S. Cowell, F. Millange, D. O'Hare, *Chem. Mater.* **2004**, *16*, 1153.
[188] F. C. Meldrum, V. J. Wade, D. L. Nimmo, B. R. Heywood, S. Mann, *Nature* **1991**, *349*, 684.
[189] T. Douglas, M. Young, *Nature* **1998**, *393*, 152.
[190] J. F. Banfield, S. A. Welch, H. Zhang, T. T. Ebert, R. L. Penn, *Science* **2000**, *289*, 751.
[191] X. Peng, *Chem. Eur. J.* **2002**, *8*, 335.
[192] I. Mekis, D. V. Talapin, A. Kornowski, M. Haase, H. Weller, *J. Phys. Chem. B* **2003**, *107*, 7454.
[193] Q. Wei, S.-Z. Kang, J. Mu, *Colloids Surf. A* **2004**, *247*, 125.
[194] E. M. Boatman, G. Lisensky, K. J. Nordell, *J. Chem. Educ.* **2005**, *82*, 1697.
[195] P. D. Cozzoli, A. Kornowski, H. Weller, *J. Am. Chem. Soc.* **2003**, *125*, 14539.

Received: January 19, 2007
Revised: March 20, 2007
Published online on June 6, 2007

